Volcano evolution and eruptive flux on the thick crust of the Andean Central Volcanic Zone: $^{40}Ar/^{39}Ar$ constraints from Volcán Parinacota, Chile

John M. Hora†
Brad S. Singer
Department of Geology and Geophysics, University of Wisconsin–Madison, 1215 W. Dayton Street, Madison, Wisconsin 53706, USA

Gerhard Wörner
Geowissenschaftliches Zentrum der Universität Göttingen, Abteilung Geochemie, Goldschmidtstrasse 1, 37077 Göttingen, Germany

ABSTRACT

The 163 k.y. history as well as the chemical and 46 km^3 volumetric evolution of Volcán Parinacota are described in detail by new mapping, stratigraphy, and 57 $^{40}Ar/^{39}Ar$ ages determined from groundmass or sanidine crystals in basaltic andesitic to rhyolitic lavas. A more precise chronology of eruptions and associated eruptive volumes of this central Andean volcano, which was built upon 70-km-thick crust, provides a more complete view of how quickly volcanic edifices are built in this setting and how their magmatic systems evolve during their lifetime. Development of the complex involved initial eruption of andesitic lava flows (163–117 ka) followed by a rhyodacite dome plateau (47–40 ka) synchronous with the onset of the building of a stratocone (52–20 ka), which was later destroyed by a debris avalanche ~3 times larger than that at Mount St. Helens in 1980. Dome plateau emplacement occurred faster and later than has previously been published, implying a compressed duration of cone building and introducing a preceding 65 k.y. hiatus. Debris avalanche timing is refined here to be older than 10 but younger than 20 ka. Rapid postcollapse rebuilding of the volcanic edifice is delineated by 16 groundmass and whole-rock $^{40}Ar/^{39}Ar$ ages, which include some of the youngest lava flows dated by this method. Increase in cone-building rate and a continued trend toward more mafic compositions following collapse imply an inter-relationship between the presence of the edifice and flux of magma from the feeding reservoir. Cone-building rates at Parinacota are similar to those at other well-dated volcanoes on thinner crust; however, the distributed basaltic volcanism prevalent in those other arcs is virtually absent both at Parinacota and elsewhere in the Central Volcanic Zone. This suggests that while the hydrous, calc-alkaline magmas that make up the central volcanoes are not significantly retarded by thick crust, primitive, dry basalts might be.

Keywords: Andes, Central Volcanic Zone, Parinacota, $^{40}Ar/^{39}Ar$ geochronology, eruptive rates.

INTRODUCTION

Subduction-zone magmas interact with the lithospheric mantle and crust of the overlying plate that must be traversed before they can erupt. Based on chemical and isotopic composition of these magmas, such interaction is expected to be more extensive in regions of thickened continental crust relative to oceanic arcs. This has been attributed to deeper stagnation of primitive magmas (Hildreth and Moorbath, 1988; Leeman, 1983) operating in addition to ubiquitous differentiation in shallow, subvolcanic plumbing systems. During ascent, magma progress through the crust is controlled both by its rheology and density contrast between it and the surrounding rock. Indeed, a large proportion of magmas crystallize within the crust, having never reached the surface. While global average rates of volcanism are lower in continental versus oceanic settings (Crisp, 1984; White et al., 2006), there is little evidence of significantly increased intrusive:extrusive ratios in continental crust (White et al., 2006). Calc-alkaline subduction-derived magmas typically contain >4% dissolved water (Grove and Kinzler, 1986; Sisson and Grove, 1993), and they have significantly decreased densities relative to dry magmas of the same composition (Ochs and Lange, 1999), making them buoyant relative to crust across their compositional spectrum. However, other factors, including the presence of the volcanic edifice itself (Pinel and Jaupart, 2000), may also contribute to crustal "filtering" of ascending magmas, even on thick Andean crust where edifice loading is <5% relative to total crustal thickness.

For those magmas that do erupt, there exists a broad spectrum of eruptive styles, indicating a variety of storage and transport regimes in the upper crust. These range from numerous, small, and usually mafic monogenetic centers, which imply many ephemeral conduits through the upper crust, to large silicic calderas, which are evidence of long repose times of magma accumulation with correspondingly voluminous magma chambers. Stratovolcanoes populate the intermediate region of this spectrum, and they represent moderate-volume, multiply reactivated magmatic systems that have protracted histories and several episodes of activity.

This study examines in detail the volumes and timing of eruption of arc magmas that have transited the entire crust and erupted at Parinacota, a central Andean volcano built upon very thick crust. Accurate quantification of time spans during which cone building took place allows us to assess the nonuniformity of eruptive flux. Comparison of cone-building rates with volcanoes built on thinner crust is a first step toward meaningful assessment of the role that crust plays as a rheological and density filter, i.e., its effect on the probability that a given magma batch will erupt. The specific goals of the study are to (1) better understand the throughput of magma in a multiply replenished subvolcanic system, (2) use that information to integrate changes in volcano morphology with magma system configuration, and (3) through comparison with cone-building rates of volcanoes on thinner crust, examine the role that the crustal column plays in modulating surface flux and peak cone-building rates. Because

†E-mail: jhora@geology.wisc.edu

GSA Bulletin; March/April 2007; v. 119; no. 3/4; p. 343–362; doi: 10.1130/B25954.1; 8 figures; 6 tables; Data Repository item 2007064.

time intervals between pulses of volcanic activity in a given region and associated magma volumes are highly variable, especially if disparate eruption types occur, (i.e., cinder cones, stratovolcanoes, and caldera-sourced ignimbrites), it is difficult to define an appropriate time and area scale at which different arcs may be compared. By reducing the problem to simply comparing cone-building rates of volcanoes that are otherwise broadly similar in size and type and by studying a time span that includes two such cone-building periods, this study endeavors to make meaningful comparisons without having to tackle the nearly intractable problem of obtaining high-precision geochronology and volumes for every volcano in the arc.

Composite stratovolcanoes are among the defining features of volcanic arcs. Due to their longevity, they can be used to examine eruptive flux at a single location through time. Subvolcanic magmatic processes have long been a focus of petrology and geochemistry. However, integrating the temporal variability and interconnectivity of the magma reservoirs involved with time scales of crystallization and magma movement (or stagnation) through parts of the system remains a frontier of igneous petrology (Davidson et al., 2005; Hawkesworth et al., 2004; Jicha et al., 2005). A complete appreciation of processes that modulate flux of magma through subvolcanic plumbing systems requires that the corresponding rates of magmatic output and magma compositions be known in detail over the lifetime of such systems. A quantitative time line is important to the development of petrogenetic models in several ways: (1) By correlating flows on different sectors of a volcano, it can provide an unambiguous sequence of magma compositions erupted, without having to rely on tenuous stratigraphic assignments for units not in contact with one another. (2) Knowledge of the duration of periods of quiescence provides greater confidence in identifying consanguineous magma batches. (3) The absence of adequate geochronology commonly results in the assignment of eruptive stages in which similar lavas are lumped together according to composition and texture, and somewhat artificially, assigned a rank in erupted sequence. Integration of vent locations and chemical composition with geochronology allows identification of multiple distinct magma batches erupting during the same time interval, yielding potentially useful information on magma system compartmentalization.

Whereas qualitative reconstructions based on historical accounts of the most recent eruptions, relative stratigraphy, or a handful of isotopic age determinations abound, there is a paucity of comprehensive eruptive chronologies for single, long-lived, volcanic systems with adequate temporal resolution to quantitatively constrain the durations of cone-building events and intervening lacunae. The few extant geochronologic studies of sufficient detail for arc volcanoes indicate that cone building occurs in relatively short-lived bursts of activity separated by periods of quiescence (Hildreth and Lanphere, 1994). Average eruption rates determined from global compilations or integrated over large segments of an arc (Crisp, 1984; White et al., 2006) are very useful for determining planetary-scale energy budgets and long-term thermal evolution of Earth. However, histories of individual volcanoes determined on the basis of only a few age determinations provide, at best an incomplete, and at worst, a wholly inaccurate view of true eruptive fluxes at any given time in a particular volcano's history.

There are, however, less than a dozen subduction-related volcanoes worldwide for which such detailed geochronologic studies are closely tied to stratigraphy, composition, and volume estimates, allowing a reasonably complete, quantitative history to be translated into meaningful eruptive flux rates. Of these, Santorini (Druitt et al., 1999), Montserrat (Harford et al., 2002), and Seguam (Jicha and Singer, 2006; Jicha et al., 2005) are stratovolcanoes built upon oceanic crust. A more extensive sampling of continental volcanoes exists, including Ceboruco–San Pedro (Frey et al., 2004), the Tequila volcanic field (Lewis-Kenedi et al., 2005), Katmai (Hildreth et al., 2003b), Mount Baker (Hildreth et al., 2003a), Mount Adams (Hildreth and Lanphere, 1994), and Tatara–San Pedro (Singer et al., 1997). However, all of these sit atop crust of average thickness (30–40 km). From these studies, peak volumetric growth rates during cone building occupy a broad range between 0.2 and 5 km^3/k.y. for late Pleistocene to Holocene volcanism.

Here, we aim to quantify for the first time the eruptive output at a major frontal arc stratovolcano in the Andean Central Volcanic Zone. We use these results to explore whether the exceptionally thick crust beneath this arc has affected magma ascent or decreased rates of cone building compared with other, more typical arcs. While on average the rates in oceanic arcs are greater relative to continental arcs amongst the volcanoes listed above, the variability among members of the same tectonic setting is so large that no robust conclusions can be drawn. We have chosen Volcán Parinacota at 18°S, 69°W, in the central Andes at the border between northernmost Chile and Bolivia (Fig. 1) for several reasons: (1) Since the Miocene, precipitation and hence vegetation and erosion have been extraordinarily sparse, thereby preserving excellent exposures and raising confidence that eruptive volumes estimates are accurate. (2) Previous geologic mapping of the complex has been published (Clavero et al., 2004; Wörner et al., 1988) and has revealed an intricate history including: a large variety of erupted compositions, shifting vent locations, catastrophic destruction by sector collapse with related debris avalanche processes, and repeated episodes of cone growth. (3) Unlike many volcanoes that have undergone sector collapse, Parinacota preserves enough precollapse stratigraphy on its southern flanks to allow broad correlation of in situ units with those in the debris field, based on age, chemistry, texture, and mineralogy. (4) Extensive geochemical and isotopic data (Clavero et al., 2004; Davidson et al., 1990; Wörner et al., 1988) indicate that Parinacota has erupted a high-K calc-alkaline magma series (2.5–4.5 wt% K_2O), thereby making even the youngest of its lavas good candidates for precise $^{40}Ar/^{39}Ar$ dating. Finally, (5) a handful of published K-Ar, $^{40}Ar/^{39}Ar$, ^{3}He, and U-Th ages indicate a life span of ~200 k.y. (Bourdon et al., 2000; Clavero et al., 2004; Wörner et al., 1988, 2000a), which makes it amenable for a more detailed $^{40}Ar/^{39}Ar$ study.

TECTONIC AND GEOLOGIC SETTING

Parinacota (~46 km^3 total erupted volume) is the younger of two stratovolcanoes that form the Nevados de Payachata complex in the Andean Central Volcanic Zone. Here, the Nazca plate, of Eocene age (Herron, 1972; Müller et al., 1997), is subducting beneath the South American plate (Fig. 1). The Central Volcanic Zone is one of four Quaternary volcanic zones in the Andes (inset Fig. 1), where the dip of the subducting lithospheric slab is relatively steep (~30°). Intervening segments of the orogen with no active volcanism overlie "flat-slab" (~5–10° dip) regions (Jordan et al., 1983). The crust of the Central Volcanic Zone is ~70 km thick (James, 1971), about double the crustal thickness of most continental arcs. In its northern portion, it contains the buried margin of the South American craton, which is composed of mid-Proterozoic metamorphic rocks (Wörner et al., 2000b) in the Parinacota region. In the southern Central Volcanic Zone, the crust is composed of Paleozoic-Mesozoic igneous and metasedimentary rocks (Lucassen et al., 2001).

Subduction has been occurring beneath the Central Volcanic Zone since Jurassic time; however, crustal thickening did not occur until Oligocene time, coincident with an increase in convergence rate and eastward shift in magmatism (Coira et al., 1982). Formation of Miocene-Pliocene stratovolcanoes and eruption of large-volume silicic ignimbrites followed the onset of crustal thickening. Eruption of the

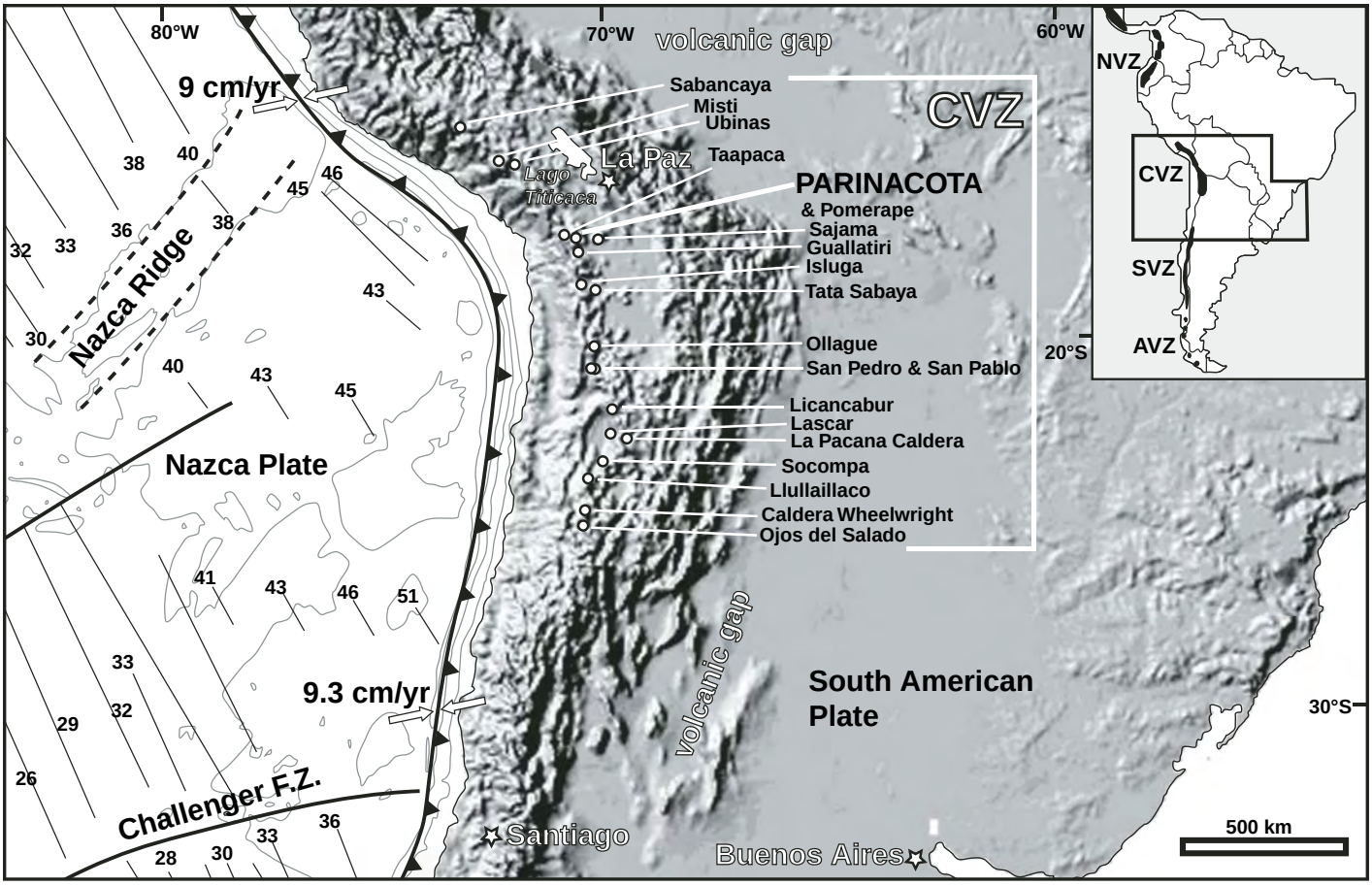

Figure 1. Digital elevation model of the Central Volcanic Zone, with major volcanic centers indicated. Seafloor ages are in Ma, correlated from magnetic anomalies (Addicott et al., 1981), and bathymetry contours represent 2000 m intervals. Inset: Location within South America with the four volcanic zones indicated: NVZ—northern volcanic zone, CVZ—Central Volcanic Zone, SVZ—southern volcanic zone, and AVZ—austral volcanic zone. F.Z.—fracture zone.

regionally important Oxaya ignimbrite occurred between 22.7 ± 0.2 and 18.6 ± 0.7 Ma (uncertainties throughout this paper are reported at 2σ) (Wörner et al., 2000a). The products of this volcanism cover the Altiplano and the slope to the Pacific Ocean. A second, regionally important tuff immediately underlying Quaternary volcanism is the 2.7 ± 0.1 (2σ) Ma Lauca ignimbrite, which also forms the basement to Parinacota (Wörner et al., 2000a).

Physiographically, the region is located at the western margin of a high (~4000 m) plateau called the Altiplano, which formed between the Eastern and Western Cordillera during the evolution of the Andean orogen (0–27 Ma). Due to the arid climate and lack of erosion, evidence of older volcanism has not been erased, and, consequently, the Central Volcanic Zone is a near-continuous belt of hundreds of partially overlapping and superimposed volcanoes of varying size, age, and eruptive duration (González Ferrán, 1995). Only a small proportion of these volcanoes has been active at any given time, meaning that spacing of active vents is not significantly different from other arcs. Parinacota is one of 44 Central Volcanic Zone stratovolcanoes that have been identified as potentially active based on Landsat Thematic Mapper image interpretation of postglacial (Holocene) activity (de Silva and Francis, 1991). Based on the data compilation by de Silva and Francis (1991), the edifice size and elevation of Parinacota are typical of most of the potentially active volcanoes in the Central Volcanic Zone.

Volcanism in the Central Volcanic Zone consists almost entirely of stratovolcanoes and large-volume silicic calderas. Most arcs worldwide have a significant component of basaltic magmas that form areally extensive fields of monogenetic, individually small cinder cones and associated lava flows. In aggregate, these distributed volcanic fields comprise a significant volumetric proportion of magma output of arcs built on thin crust. In the modern Central Volcanic Zone, they are nearly absent, suggesting a fundamental difference between it and other arcs. In the Cascade arc, for example, two distinct types of magma with disparate source regions have been identified, corresponding to the focused versus distributed volcanism (Grove et al., 2002; Elkins Tanton et al., 2001). Magmas that contribute to the distributed volcanism are dry and tholeiitic and were produced between 36 and 66 km depth in the uppermost mantle due to the vertical component of wedge corner flow (Elkins Tanton et al., 2001), whereas the hydrous calc-alkaline magmas contributing to focused volcanism were generated in the mantle directly above the downgoing slab (Grove et al., 2002). It would appear that in the modern Central Volcanic Zone, the dry tholeiites are either not produced in any significant quantity, or they fail to reach the surface.

VOLCANOLOGICAL OVERVIEW

Parinacota (6350 m) and Pomerape (6222 m), an older adjacent glacially eroded stratocone, together comprise the Nevados de Payachata.

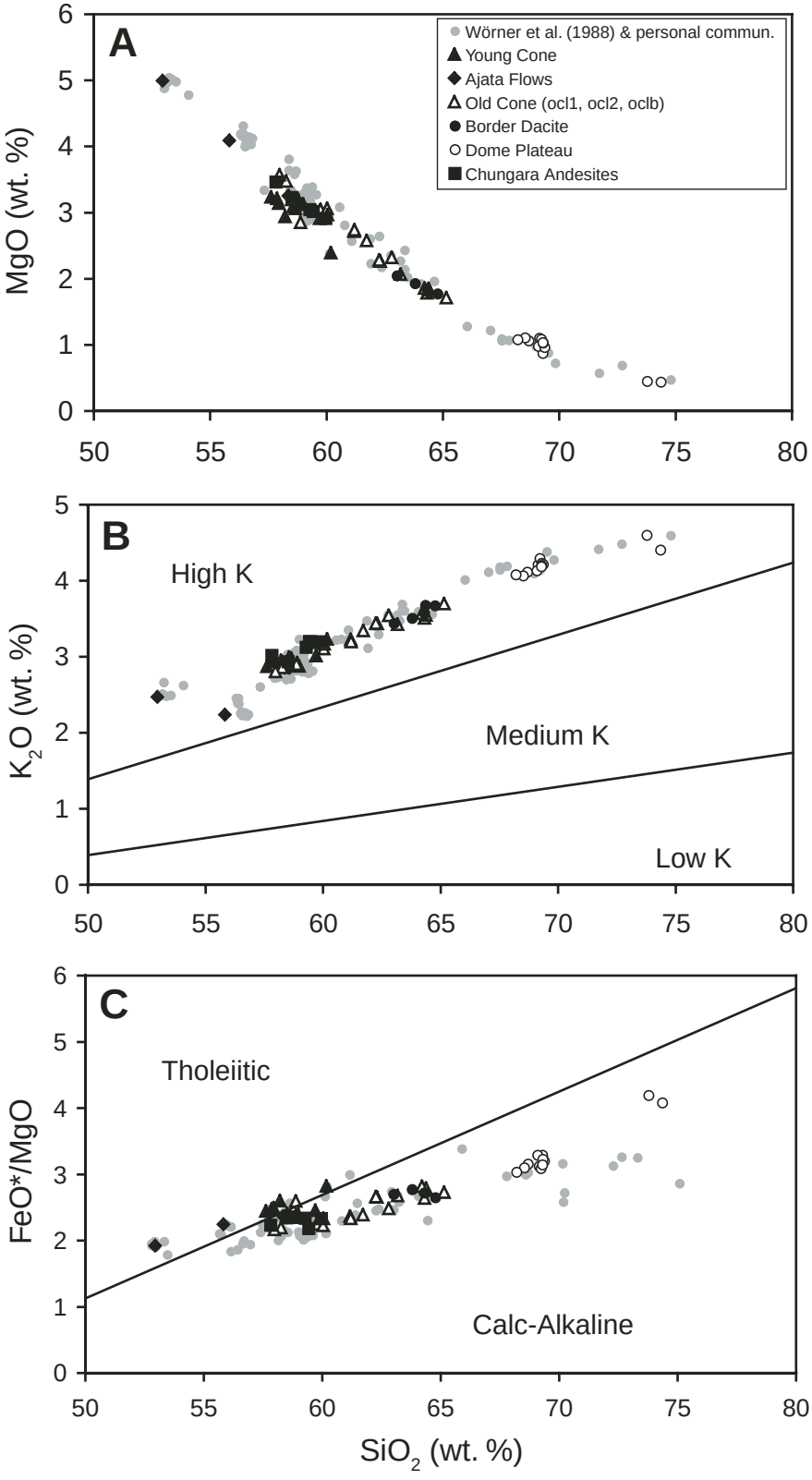

Figure 2. MgO, K_2O, and FeO*/MgO versus SiO_2 (wt%) for all dated Parinacota samples (prominent symbols) and previously analyzed samples from Wörner et al. (1988) and Wörner (2006, personal commun.). Data are from X-ray fluorescence (XRF) at the University of Göttingen using the methods of Hinners et al. (1998).

Erupted lavas range from basaltic andesite to rhyolite (Fig. 2), yet no simple monotonic progression with age is evident from the previous stratigraphic and geochemical studies (Clavero et al., 2004; Davidson et al., 1990; Wörner et al., 1988). Lavas of the first eruptive stage comprise at least 4 km^3 of plagioclase and two pyroxene phyric Chungará andesites, which form an ~50-m-high multilobed flat plateau along the northern margin of the depression now occupied by Lago Chungará at 4540 m above sea level (asl). Atop these is a field of partially coalesced rhyodacitic domes (Dome Plateau) that were erupted from multiple vents. The exact number and location of vents are unknown since multilobed domes are not asymmetrical due to preferential flow in a given direction, and a large part of the plateau's original areal extent was removed by the collapse event later in the volcano's history. After formation of the Dome Plateau, onset of major cone building began to the northeast and formed a stratocone composed mostly of hornblende and biotite-bearing andesite and dacite, here called the "Old Cone."

This ancestral stratocone collapsed to form an ~6 km^3 debris avalanche that is ~3 times larger than the 1980 Mount St. Helens debris avalanche and was first identified in Landsat imagery by Francis and Wells (1988) and described in detail by Clavero et al. (2002). It traveled ~20 km down the Lauca valley, dammed the upper portion of the drainage, and resulted in the formation of Lago Chungará to the south of the volcano. Subsequently, the cone was rebuilt (~15 km^3), to the point of obscuring the Old Cone avalanche scarp and resulting in a completely symmetrical Young Cone edifice, with a shift toward more mafic two-pyroxene olivine basaltic andesite to andesite composition (Fig. 2) . The most recent volcanism is a series of three flank vents to the south of the main summit, which produced monogenetic cinder cones and associated Ajata flows (~0.2 km^3) of basaltic to basaltic andesite composition.

While there is general agreement regarding the sequence of events in building this volcano, the precise timing of each eruptive phase is still poorly defined, mainly because only a few relatively imprecise ages, including six whole-rock K-Ar (Wörner et al., 1988), five whole-rock or biotite $^{40}Ar/^{39}Ar$ (Clavero et al., 2004), and five ^{3}He surface exposure ages (Wörner et al., 2000a), have been determined for Parinacota and associated Ajata lava flows. These data are insufficient to precisely identify eruptive episodes and to reconstruct eruption rates, primarily because the amount of time that elapsed between major eruptive pulses in the early part of the volcano's history is not known. In particular, there is considerable uncertainty concerning the age of the spatially and stratigraphically contiguous lavas

TABLE 1. SUMMARY OF PREVIOUS STRATIGRAPHIC DIVISION OF UNITS AT VOLCÁN PARINACOTA

Stage[†]	Definition[†]	Age[†]	Stage[‡]	Definition[‡]	Age[‡]
V	Ajata vents	7 ka–recent	3	New cone, mainly formed by andesitic lava flows, pyroclastic flow and fallout deposits and lahar deposits. Simultaneous (6–1.4 ka) formation of the flank Ajata centers (basaltic andesite to andesite composition). Youngest eruptions originated from the central cone (forming pyroclastic flows and tephra fallout).	<8 ka
IV	Young cone (no amphibole)	Recent			
III	Debris avalanche with dacite bombs and Plinian pumice	13.5 ka	2	Ancestral Parinacota stratocone, mainly formed by andesitic lava flows (amph-rich and two-pyroxene) and pyroclastic fallout deposits. End of unit occurred with the collapse of the edifice at 8 ka, generating the Parinacota debris avalanche deposit.	70–8 ka
II	Old Cone dacite-andesite flows				
		53–12 ka			
		53–18 ka[§]	1	Rhyolitic to rhyodacitic domes and their associated block and ash flow deposits; andesitic and dacitic lavas and dacitic lava coulees.	300–70 ka
Ib	Rhyolite domes and associated block and ash flows	112 ka			
Ia	Chungará andesites	264–110 ka			

[†]From Wörner et al. (1988).
[‡]From Clavero et al. (2004).
[§]New data from Wörner et al. (2000).

of the rhyodacite Dome Plateau, since the four previous age determinations range from 76 ± 16 to 308 ± 24 ka, which poorly constrains how quickly the two subsequent cones (pre- and postavalanche) were built. Two proposed schemes of Wörner et al. (1988) and Clavero et al. (2004) for subdividing the stratigraphy are shown in Table 1.

Prior to this study, the whole-rock chemistry and isotopic composition of lavas erupted at Parinacota had been determined by Wörner et al. (1988), Davidson et al. (1990), Entenmann (1994), and Bourdon et al. (2000). The Nevados de Payachata lava flows define a continuous high-K calc-alkaline trend (Figs. 2B and 2C), which is typical of most Central Volcanic Zone volcanoes, but they are enriched in Sr, Ba, and Ti relative to older Miocene lavas erupted in the region (McMillan et al., 1993). The lavas show an isotopic shift from typical mantle values toward crustal compositions, indicating up to 20% of deep crustal assimilation (Davidson et al., 1990). However, overall, there is a restricted range in Sr and Nd isotopic ratios, suggesting that assimilation had a negligible effect during shallow magmatic differentiation. One of the Ajata flow lavas has the lowest $^{87}Sr/^{86}Sr$ in the volcanic complex and is very rich in Sr (up to 1700 ppm) and Ba (up to 1800 ppm), representing a chemical signature unusual in the Central Volcanic Zone. Linear trends in Harker diagrams (e.g., Figs. 2A and 2B) versus limited deviation from a hyperbolic fractional-crystallization trend on a Ni-Rb plot led Wörner et al. (1988) and Davidson et al. (1990) to suggest that Old Cone magmas are dominated by fractional crystallization, while the Young Cone lavas show increased mixing.

Ginibre et al. (2002a, 2002b) studied plagioclase zoning and analyzed trace-element compositions in growth zones spanning resorption horizons with high spatial resolution from one of the more evolved Old Cone dacite coulees. Two types of crystals were found: one records intrachamber mixing of the host magma with a more evolved boundary layer, while the second type records mixing of the host magma with crystal cores sourced in magmas similar to two distinct compositions present in the Ajata flows. This corroborates the hypothesis of intratrend mixing during the Old Cone portion of the volcano's history and implies that two types of basaltic magmas equivalent to the high-Sr and low-Sr Ajata flows were present in the magmatic system long before magmas of those compositions erupted from the Ajata satellite vents.

METHODS

Field Studies

Sampling of representative volcanic units was carried out both on the volcanic edifice and debris avalanche. We focused on the southern half of the edifice, since the greatest variability in age and chemistry of erupted lavas is found there (Clavero et al., 2004; Wörner et al., 1988). Access to the volcanic cone was mostly on foot from several 4 × 4 tracks that approach the base of the volcano near the northeast shore of Lago Chungará and traverse the debris avalanche between Lagunas Cotacotani and the volcano. Field relationships were mapped (Fig. 3) onto a 1:50,000 topographic base (IGM 1800-6900 Volcán Parinacota sheet), guided by the geologic map of Clavero (2002).

The northeast and northwest sectors of the map are largely unaltered from Clavero (2002), although some map units have been reassigned based on the geochronology of this study. Significant new mapping was done on the southern half of the edifice, coincident with sampling for geochronology. The map presented here (Fig. 3) differs from Clavero (2002) in these areas; we show more underlying geology, rather than emphasizing thin pyroclastic cover, and likewise, new field observations and age determinations necessitated reassignment of some units.

The volcanic units shown in the geologic map (Fig. 3) consist of lava flows, coulees, and domes, as well as units associated with the debris avalanche. Pyroclastic flow, fall, and lahar deposits associated with the Young Cone are shown only where their interpreted thickness is large enough to preclude interpretation of underlying geology. Individual flow units have been shown separately where feasible, but several units (e.g., ca, ocl1, ocl2, ycl, and ycp) include all flows in a given age and chemistry range. Individual flows (e.g., ocb, d2, d3) were correlated on the basis of indistinguishable age and major-element chemistry.

Volume Estimation

Volume estimates for in situ units were done by partitioning the volume under present topography using geologically reasonable assumptions regarding locations of contacts at depth. Due to aridity, erosion by water on the Altiplano is negligible; however, it is important to note that wind-dispersed distal tephras sourced at Parinacota are not included in the volume calculations, and, therefore, the estimates presented in this paper should be regarded as minimum volumes. Volume estimates for the debris avalanche are taken from Clavero et al. (2002), as that study focused on the debris avalanche and its mechanism of emplacement. A full description of volume calculations for units that make up the edifice, and assumptions associated with

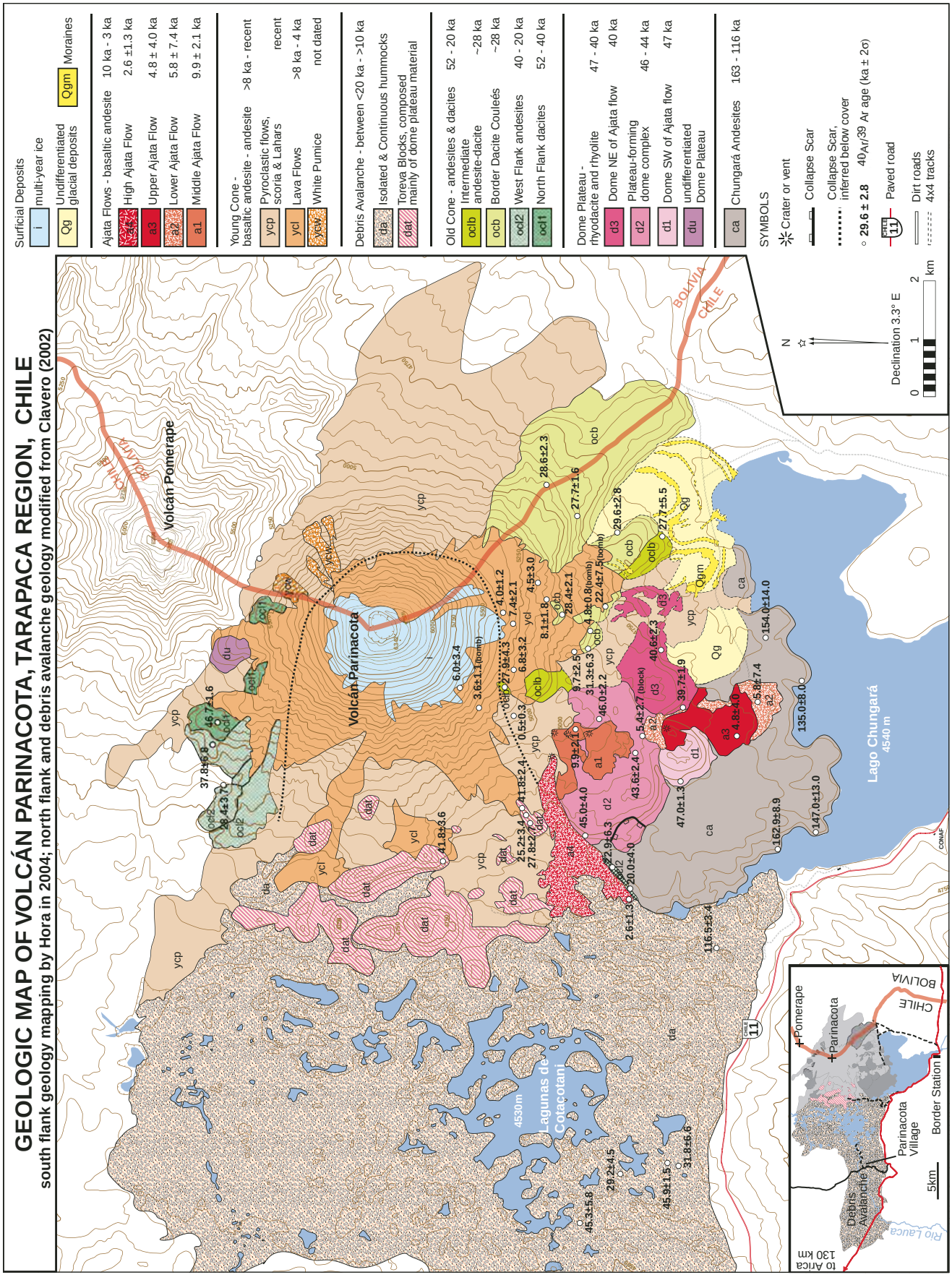

Figure 3. Geologic map of Volcán Parinacota, revised from Clavero (2002) and based on new geochronology and field relations.

those calculations, is given in the GSA Data Repository and associated Figure DR1.[1]

$^{40}Ar/^{39}Ar$ METHODS

Sample Preparation

Target phases for geochronology were sanidine or holocrystalline groundmass for phyric samples lacking sanidine. For a few aphyric samples, whole-rock cores 5 mm in diameter and ranging from 80 to 750 mg were drilled from hand specimens. Sanidine >500 μm was readily handpicked from coarsely crushed samples and separated from plagioclase via heavy liquids adjusted to 2.63 g/cm^3. Final selection of grains was done under binocular microscope. For step-heating analysis, sanidines of ~5–30 mg were used. For sanidine crystals ≤5 mg, only single-crystal total fusions were done. Groundmass aliquots of 75–350 mg were separated from the 250–500 μm size fraction of crushed samples by magnetic and heavy liquid separation of crystalline phases, which could potentially host extraneous argon; this was followed by handpicking and encapsulation in pure Cu foil packets.

Cu packets, whole-rock wafers, and sanidine crystals were placed into wells in 2.5-cm-diameter Al disks interspersed with 9–15 crystals of 1.194 ± 0.012 Ma Alder Creek Rhyolite sanidine (Renne et al., 1998) as a neutron flux monitor. Up to eight Al disks were assembled into a cylindrical stack and irradiated in the cadmium-lined in-core irradiation tube (CLICIT) at the Oregon State University TRIGA reactor for 20 or 30 min. Fast neutron doses were typically 1.2–1.8 × 10^{15} n/cm^2. Corrections for undesirable nucleogenic reactions on ^{40}K and ^{40}Ca are as follows: $[^{40}Ar/^{39}Ar]_K$ = 0.00086; $[^{36}Ar/^{37}Ar]_{Ca}$ = 0.000264; and $[^{39}Ar/^{37}Ar]_{Ca}$ = 0.000673 (Singer et al., 2004). J values were uniform within analytical error across individual Al disks, but varied significantly between disks, with 1σ uncertainties between 0.55% and 1.30%. This uncertainty in the value of J was propagated in age calculations for each sample, but contributes less than 1% of the overall age uncertainty for the young materials measured here. The age uncertainty determined for each sample is the 2σ analytical error, unless otherwise noted.

Gas Extraction and Mass Spectrometry

At the University of Wisconsin–Madison Rare Gas Geochronology Laboratory, groundmass and whole-rock samples were incrementally heated in a double-vacuum resistance furnace or, in the case of sanidine, by 25 W CO_2 laser. Prior to each furnace step-heating experiment, samples were heated at 450–650 °C and pumped to remove potentially large amounts of water and atmospheric Ar. Numerous tests revealed that gas released at these temperatures liberated only negligible amounts (<1%) of the total ^{39}Ar, and, therefore, omitting this gas from the experiment was of little consequence to age determination, and a far greater benefit was gained from not polluting the extraction line for subsequent steps. Experiments consisted of 5 to 15 steps in the temperature interval between 650 and 1400 °C. Each incremental heating step consisted of a 2 min ramp time for the furnace to reach the desired temperature, which was then maintained for 10–15 min. During the heating time, and for an additional 7–8 min afterward, the sample gas was exposed to three SAES C50 Zr-Al getters attached to the 300 cm^3 extraction line. Step heating of sanidine used a defocused beam from the CO_2 laser that was rastered over crystals larger than 5 mg for 2–4 min. This study benefits from the large size of Dome Plateau sanidine crystals (~1–3 mm), so that individual grains were step heated in experiments of ≥5 steps, rather than relying on data from a mixed population of old and juvenile grains. From some samples, several crystals of sanidine smaller than 5 mg were also fused individually, and the gas was measured for an age determination. Gas cleanup time following laser heating was typically 3 min.

Isotopic analysis of all samples in a MAP 215-50 mass spectrometer followed procedures of Singer et al. (2004), with data reduction via ArArCALC software (Koppers, 2002). Accurate dating of late Pleistocene–Holocene samples is highly dependent on procedural blanks and instrumental mass discrimination corrections (e.g., Singer et al., 2004). Prior to sample introduction, furnace blanks were measured at 200 °C increments throughout the temperature range spanned by the incremental heating and interpolated. Mass discrimination was monitored daily via an automated air pipette and varied between 1.0022 and 1.0077 per atomic mass unit (a.m.u.) during the analytical period. To improve precision, nearly all age determinations were repeated at least once.

$^{40}Ar/^{39}Ar$ RESULTS

Results of $^{40}Ar/^{39}Ar$ age determinations on 57 samples, based on 124 incremental heating analyses (done either by furnace or laser) and 90 single-crystal laser fusion (SCLF) analyses are reported in Tables 2, 3, and 4, and representative age spectra and inverse isochrons are shown in Figure 4. Table 2 summarizes the furnace and laser step-heating results, whereas Table 3 summarizes the SCLF data. For samples on which both types of analysis (incremental heating and SCLF) were done, each plateau age or fusion age was treated as an independent measurement, an inverse-variance weighted mean apparent age was calculated, and the resulting ages are reported in Table 4. The combined isochron ages and $^{40}Ar/^{36}Ar$ values calculated for these samples used fusion ages and steps from plateau segments to define the regressions. Complete results are given in Tables DR1 and DR2 (see footnote 1).

Furnace heating of 117 groundmass or whole-rock aliquots only yielded detectable radiogenic argon in 72 cases; only these are considered successful and are included in the previous total—those found to contain <1% total radiogenic argon were not considered further. The majority of samples gave inverse isochron $^{36}Ar/^{40}Ar$ intercepts within 2σ of the atmospheric value, and because there is no evidence for excess argon, the plateau ages give the most precise age for these samples. Nine samples had nonatmospheric $^{36}Ar/^{40}Ar$ intercepts, and many of these also had weakly saddle-shaped spectra (e.g., Fig. 4, PAR-03-39), suggesting that a small amount of excess argon was present (Lanphere and Dalrymple, 1976; McDougall and Harrison, 1999). For these few samples, the isochrons give the most precise and accurate age since they are independent of the assumption of an atmospheric trapped argon component.

Sanidine phenocrysts (52 laser incremental heating and 108 SCLF) typically yielded more precise ages than groundmass, reflecting much higher K_2O and thus radiogenic argon contents (e.g., Fig. 5A). Analysis of phenocrysts, however, introduces the possibility of contamination with extraneous argon (e.g., Singer et al., 1998). Incremental heating of a small number of large (~5 mg) biotite crystals (Fig. 5B) from Dome Plateau lavas indicates that while sanidine yields tightly clustered ages in accord with stratigraphic position, the apparent ages of the biotite crystals are significantly older (Fig. 5B). These anomalously old biotite ages are: (1) discordant with the sanidine from the same hand specimen, (2) scattered over several hundred thousand years in a single hand specimen for which several crystals were measured, and (3) in conflict with the stratigraphy of the sample sites and ages determined from under- and overlying units. This calls into question the usefulness of the whole-rock K-Ar age of 112 ka age reported in Wörner et al. (1988) and the $^{40}Ar/^{39}Ar$ ages on biotite and hornblende (76.2 ± 16.4 ka, 302.9 ± 14.2 ka, 308.0 ± 24.0 ka, and 138.9 ± 42.8 ka) reported by Clavero et al. (2004). One likely cause of extraneous argon is

[1]GSA Data Repository item 2007064, Tables DR1–DR3 and Figure DR1, is available on the Web at http://www.geosociety.org/pubs/ft2007.htm. Requests may also be sent to editing@geosociety.org.

TABLE 2. SUMMARY OF $^{40}Ar/^{39}Ar$ INCREMENTAL-HEATING EXPERIMENTS*

Sample	Map unit§	Latitude (S)	Longitude (W)	Material#	No. of exp.	Age spectrum					Total fusion age (ka ± 2σ)	Isochron analysis##		
						Plateau age** (ka ± 2σ)*	Increments†† used (°C)	^{39}Ar %	*N*§§	MSWD		$^{40}Ar/^{36}Ar_i$ (±2σ)	Age (ka ± 2σ)	MSWD
Ajata flows														
PAR-03-25***	a4	18°11.820′	69°11.410′	gm	3	6.6 ± 1.6	600–1280	86.9	19 of 24	2.70	9.6 ± 2.0	299.6 ± 2.7	**2.6 ± 1.3**	0.71
PAR-222	a3			gm	1	***4.8 ± 4.0***	1115–1370	73.1	6 of 12	0.39	5.0 ± 3.3	296.5 ± 5.6	1.8 ± 2.6	0.46
PAR-219	a2			gm	1	***5.8 ± 7.4***	950–1175	70.9	4 of 6	0.21	5.3 ± 6.1	296.9 ± 4.3	0.3 ± 1.2	0.10
PAR-03-20	a1	18°11.747′	69°09.566′	gm	3	10.2 ± 1.8	650–1250	92.3	19 of 25	1.30	16.7 ± 3.3	298.3 ± 2.5	**5.4 ± 2.7**	0.61
PAR-03-19	a1	18°11.627′	69°09.582′	gm	2	***9.9 ± 2.1***	600–1150	89.3	9 of 13	1.20	13.5 ± 2.3	296.6 ± 4.0	8.0 ± 5.5	0.58
Young Cone														
PAR-03-43	ycl	18°11.211′	69°09.311′	gm	2	6.2 ± 2.1	600–1250	91.6	13 of 16	1.30	11.1 ± 2.6	299.4 ± 3.3	**0.5 ± 0.3**	0.81
PAR-03-39	ycp	18°10′	69°09′	wr	3	3.8 ± 1.1	700–1350	85.6	18 of 20	2.20	7.3 ± 2.2	300.7 ± 4.3	**3.6 ± 1.1**	1.27
PAR-03-14	ycl	18°10.966′	69°08.477′	wr	2	***4.0 ± 1.2***	825–1400	87.8	9 of 12	0.26	9.0 ± 8.6	297.9 ± 5.0	3.3 ± 1.2	0.98
PAR-129	ycp			gm	2	***4.3 ± 2.6***	925–1475	85.7	11 of 13	0.00	4.7 ± 2.6	298.7 ± 4.8	0.9 ± 0.6	1.08
PAR-04-09	ycl	18°11.444′	69°08.065′	gm	1	***4.5 ± 3.0***	900–1200	82.1	5 of 10	0.68	10.7 ± 3.3	295.6 ± 4.0	4.2 ± 4.1	0.90
PAR-03-15	ycl	18°11.243′	69°08.549′	gm	2	9.7 ± 2.5	700–1350	94.5	21 of 23	0.13	13.6 ± 3.1	298.0 ± 1.7	**4.6 ± 2.6**	0.40
PAR-04-12	ycp	18°11.749′	69°08.600′	wr	2	***4.8 ± 0.8***	1050–1350	47.3	7 of 17	2.20	27.9 ± 1.4	316.3 ± 40.2	3.1 ± 1.9	1.58
PAR-03-38	ycl	18°10.512′	69°09.083′	gm	2	11.0 ± 3.0	600–1325	96.2	13 of 17	0.13	17.7 ± 4.5	297.8 ± 1.8	**6.0 ± 3.4**	0.54
PAR-03-34	ycl	18°11.428′	69°08.823′	gm	3	***6.8 ± 3.2***	675–1325	63.5	13 of 27	1.20	16.2 ± 3.8	296.7 ± 2.3	2.8 ± 1.7	1.39
PAR-03-12	ycl	18°11.058′	69°08.529′	wr	2	***7.4 ± 2.1***	700–1460	94.2	12 of 14	1.30	10.0 ± 2.3	298.0 ± 2.9	7.0 ± 1.8	1.95
PAR-04-10	ycl	18°11.421′	69°08.339′	gm	2	***8.1 ± 1.8***	800–1300	87.7	8 of 14	0.29	11.3 ± 1.8	297.7 ± 3.2	5.2 ± 3.6	0.52
Old Cone (including Border Dacite)														
PAR-082	ocl2	18°11.167′	69°10.167′	gm	2	***20.0 ± 4.0***	925–1260	86.9	9 of 11	1.40	17.3 ± 5.2	295.9 ± 3.6	19.4 ± 7.1	0.93
PAR-04-13	oce	18°11.861′	69°08.328′	wr	3	31.6 ± 5.8	800–1450	66.2	17 of 38	1.90	53.0 ± 8.3	297.6 ± 1.7	**22.4 ± 7.5**	0.93
PAR-03-28	ocl2	18°12.083′	69°11.114′	gm	3	***22.9 ± 6.3***	675–1260	75.2	17 of 28	0.16	39.7 ± 8.0	297.1 ± 2.2	9.2 ± 4.7	0.96
DBF-03-05	oclb/da	18°11.746′	69°15.165′	gm	2	***23.0 ± 3.5***	650–1100	75.7	10 of 18	0.92	25.4 ± 10.7	295.9 ± 1.9	21.5 ± 6.9	0.84
PAR-03-03	oclb/dat	18°11.179′	69°10.424′	gm	2	***25.2 ± 3.4***	825–1350	95.0	12 of 16	1.04	28.8 ± 4.1	297.0 ± 2.0	20.6 ± 6.2	0.88
PAR-04-07	oclb	18°12.502′	69°07.726	san	2	***27.7 ± 5.5***	1.5–12 W	98.2	9 of 10	0.06	27.6 ± 8.8	296.1 ± 4.1	27.9 ± 5.5	0.16
PAR-03-05	ocb	18°11.403′	69°07.068	san	2	***27.7 ± 1.6***	1.5–9 W	99.4	9 of 10	2.10	29.1 ± 2.8	296.0 ± 6.6	27.8 ± 1.8	0.51
PAR-03-02	oclb/dat	18°11.224′	69°10.480′	gm	2	***27.8 ± 2.7***	700–1400	100.0	13 of 13	0.05	27.4 ± 3.7	295.2 ± 2.2	28.4 ± 4.6	0.45
PAR-03-36	oclb	18°11.879′	69°08.463′	gm	2	33.4 ± 3.2	700–1200	88.0	13 of 17	0.56	45.1 ± 4.1	297.8 ± 1.5	**27.9 ± 4.3**	0.81
PAR-03-09	ocl2	18°08.331′	69°10.102′	gm	2	***28.4 ± 3.7***	650–1280	91.1	15 of 21	2.10	41.5 ± 5.9	295.7 ± 1.4	27.6 ± 7.0	0.65
PAR-04-11	ocb	18°11.457′	69°08.401′	san	2	***28.4 ± 2.1***	3–10.5 W	86.4	12 of 21	2.20	34.1 ± 3.3	294.9 ± 4.3	28.8 ± 2.6	1.00
PAR-03-06	ocb	18°11.572	69°07.458′	san	2	***28.6 ± 2.3***	1.5–10.5 W	97.9	9 of 10	0.12	27.3 ± 5.2	295.1 ± 2.4	28.7 ± 2.4	0.25
DBF-03-04	ocl2/da	18°12.616′	69°14.012′	gm	2	***29.2 ± 4.5***	825–1375	94.0	10 of 15	0.48	29.3 ± 6.5	295.5 ± 1.9	29.2 ± 7.0	0.71
PAR-03-07	ocb	18°11.953′	69°07.659′	gm	2	***29.6 ± 2.8***	850–1350	94.0	9 of 13	0.00	31.5 ± 4.9	297.4 ± 2.3	26.0 ± 5.1	0.11
DBF-04-03	ocb/da	18°13.106′	69°16.458′	gm	2	***31.1 ± 1.6***	725–1260	80.5	12 of 18	2.10	38.1 ± 2.1	295.7 ± 2.0	30.8 ± 2.9	1.11
DBF-03-03	ocl2/da	18°12.950′	69°13.569′	gm	3	***31.8 ± 6.6***	775–1300	84.5	17 of 26	0.13	43.5 ± 18.7	296.3 ± 2.0	24.9 ± 12.5	0.47
PAR-03-11	ocl2	18°08.044′	69°09.831′	gm	2	***37.8 ± 6.8***	700–1350	98.9	21 of 22	1.10	39.4 ± 11.6	296.8 ± 1.6	27.8 ± 10.5	0.70
PAR-03-10	ocl1	18°08.176′	69°09.787′	san	3	***46.7 ± 1.6***	3–10.5 W	96.2	12 of 15	0.04	44.4 ± 2.5	294.3 ± 2.9	47.3 ± 2.2	0.19
DBF-03-11†	ocl1/da	18°13.286′	69°15.620′	san	3	***52.4 ± 5.4***	3–8.25 W	77.9	10 of 12	1.80	58.0 ± 6.2	345.5 ± 117.9	47.8 ± 9.9	0.84
Dome Plateau														
PAR-04-02	d3	18°12.733′	69°09.279′	san	2	***39.7 ± 1.9***	1.5–9 W	98.1	9 of 10	0.41	38.3 ± 2.8	294.6 ± 2.6	40.2 ± 2.4	0.22
PAR-04-06	d3	18°12.442′	69°08.702′	san	3	***40.6 ± 2.3***	1.5–10.5 W	100.0	13 of 13	0.42	40.4 ± 4.6	295.9 ± 3.2	40.4 ± 2.8	0.32
PAR-03-04†	du/dat	18°11.134′	69°10.368′	san	4	***43.0 ± 10.0***	3–8.25 W	93.7	15 of 16	3.90	44.0 ± 6.9	295.3 ± 3.3	42.8 ± 4.4	1.67
PAR-03-23†	du/dat	18°10.421′	69°10.897′	san	5	***43.4 ± 2.2***	3–8.25 W	91.0	17 of 20	1.10	46.8 ± 2.7	296.4 ± 5.2	43.2 ± 2.6	0.65
DBF-03-08†	du/da	18°13.292′	69°15.466′	san	5	43.4 ± 2.4	3–8.25 W	76.9	14 of 20	1.60	56.9 ± 2.3	313.7 ± 11.6	**44.0 ± 2.4**	1.09
PAR-04-01	d2	18°12.054′	69°10.852′	san	2	***45.0 ± 4.0***	3–10.5 W	96.4	8 of 10	0.28	43.8 ± 8.3	296.0 ± 2.3	44.2 ± 5.0	0.37
DBF-03-06	du/da	18°11.556′	69°14.583′	san	2	***45.3 ± 5.8***	3–10.5 W	88.9	6 of 10	0.01	100.6 ± 41.6	301.6 ± 26.7	44.1 ± 8.0	0.18
PAR-03-18†	d2	18°12.220′	69°09.642′	san	5	***45.5 ± 2.8***	2.25–8.25 W	99.7	22 of 24	2.00	41.2 ± 6.4	295.4 ± 3.4	46.2 ± 3.3	1.21
PAR-04-04	d2	18°11.947′	69°09.474′	san	1	***46.0 ± 2.2***	3–10.5 W	99.5	8 of 10	0.00	48.1 ± 3.4	297.6 ± 3.3	45.6 ± 2.4	0.31
DBF-03-02†	du/da	18°12.950′	69°13.569′	san	3	***46.3 ± 1.6***	3–8.25 W	84.0	10 of 12	1.11	55.3 ± 2.7	298.2 ± 8.8	45.8 ± 2.1	0.96
PAR-03-26	d1	18°12.675′	69°10.077′	san	4	***47.0 ± 1.3***	3–10.5 W	89.1	15 of 23	1.29	50.7 ± 1.6	300.5 ± 7.2	46.5 ± 1.5	1.21
Chungará andesites														
DBF-03-07	ca/da	18°13.183′	69°11.542′	wr	2	***116.5 ± 3.4***	700–1400	100.0	21 of 21	0.06	118.0 ± 13.2	295.3 ± 1.7	117.1 ± 6.5	0.46
PAR-03-22	ca	18°13.764′	69°09.132′	gm	2	***135.0 ± 8.0***	775–1375	94.8	20 of 23	0.33	141.1 ± 10.3	296.2 ± 2.0	129.4 ± 19.1	0.70
PAR-03-30	ca	18°13.868′	69°10.600′	gm	2	***147.0 ± 13.0***	775–1185	100.0	21 of 23	2.20	154.1 ± 18.2	296.5 ± 2.5	131.6 ± 37.8	0.47
PAR-074	ca	18°11.917′	69°09.133′	gm	2	***154.0 ± 14.0***	875–1330	95.1	14 of 18	2.40	140.4 ± 16.1	292.8 ± 3.4	181.5 ± 36.3	0.42
PAR-03-31	ca	18°13.596′	69°10.746′	gm	2	***162.9 ± 8.9***	720–1375	90.9	23 of 26	0.88	154.4 ± 13.4	296.5 ± 1.8	156.5 ± 14.1	1.66

Note: MSWD—mean square of weighted deviations. Preferred ages are in bold.

*Ages were calculated relative to 1.194 Ma Alder Creek Rhyolite sanidine (Renne et al., 1998); uncertainties are reported at 2σ precision.

†Samples for which both incremental-heating and single-crystal total fusions were done; only incremental heating results are reported here.

§Samples collected from the debris avalanche are noted xxx/da or xxx/dat, where xxx is the chemically correlated unit and da indicates debris avalanche and dat indicates Toreva block.

#Abbreviations: gm—groundmass; wr—whole rock; san—sanidine.

**Weighted mean of plateau ages from individual experiments; weighted by uncertainty only.

††Temperatures reported for resistance furnace experiments only, otherwise laser power in watts.

§§Number of data points used in isochron calculation; each incremental-heating step represents one data point.

##Data from all experiments combined, resulting in a single regression line.

***Data from sample PAR-03-25 combined with sample PAR-086 collected by G. Wörner at same locality.

TABLE 3. SUMMARY OF $^{40}Ar/^{39}Ar$ SINGLE-CRYSTAL LASER TOTAL FUSIONS OF SANIDINE

Sample	Map unit*	Latitude (S)	Longitude (W)	*N*†	Apparent ages		Isochron analysis		
					Weighted mean age (ka ± 2σ)§	MSWD	$^{40}Ar/^{36}Ar_i$ (±2σ)	Age (ka ± 2σ)	MSWD
Old Cone (including Border Dacite)									
PAR-03-16	ocb	18°11.385′	69°08.529′	9 of 13	***31.3 ± 6.3***	1.01	295.1 ± 6.2	31.8 ± 8.4	1.16
DBF-03-10	ocl1 / da	18°13.286′	69°15.620′	4 of 5	***39.0 ± 3.0***	1.60	294.7 ± 14.5	39.4 ± 6.2	2.22
DBF-03-09	ocl1 / da	18°13.344′	69°15.545′	10 of 15	***45.2 ± 1.9***	0.42	304.1 ± 19.3	43.6 ± 4.2	0.34
DBF-03-01	ocl1 / da	18°13.320′	69°15.478′	14 of 15	***48.0 ± 5.0***	0.48	294.7 ± 4.1	48.6 ± 5.9	0.51
DBF-03-11#	ocl1 / da	18°13.286′	69°15.620′	11 of 11	***52.3 ± 3.3***	1.30	366.4 ± 79.4	41.8 ± 10.2	0.91
Dome Plateau									
PAR-03-17	du / da	18°13.725′	69°20.054′	3 of 3	***29.4 ± 6.1***	1.30	299.1 ± 32.2	28.5 ± 11.8	2.45
PAR-03-23#	du / dat	18°10.421′	69°10.897′	7 of 9	***34.1 ± 4.5***	1.90	312.8 ± 89.1	30.6 ± 13.7	2.14
PAR-03-18#	d2	18°12.220′	69°09.642′	8 of 9	***37.7 ± 4.9***	0.66	295.0 ± 5.3	38.2 ± 7.2	0.76
PAR-03-04#	du / dat	18°11.134′	69°10.368′	9 of 9	***40.4 ± 3.7***	0.54	297.1 ± 4.8	38.6 ± 6.4	0.55
DBF-03-02#	du / da	18°12.950′	69°13.569′	5 of 9	***41.0 ± 5.4***	0.28	289.1 ± 14.3	42.5 ± 6.4	0.14
DBF-03-08#	du / da	18°13.292′	69°15.466′	10 of 10	***49.8 ± 2.4***	1.30	312.7 ± 59.9	45.6 ± 14.0	1.19

Note: MSWD—mean square of weighted deviations.
*Samples collected from the debris avalanche are noted xxx/da or xxx/dat, where xxx is the chemically correlated unit and da indicates debris avalanche and dat indicates Toreva block.
†Number of total fusions included in statistics in following columns.
§Ages were calculated relative to 1.194 Ma Alder Creek Rhyolite sanidine (Renne et al., 1998); uncertainties are reported at 2σ precision.
#Sample for which step-heating analysis was also done; data reported here are only for total fusions.

TABLE 4. COMBINED SUMMARY OF TOTAL FUSION AND INCREMENTAL-HEATING EXPERIMENTS ON SANIDINE FOR WHICH BOTH TYPES OF ANALYSIS WERE DONE

Sample	Map Unit*	Latitude (S)	Longitude (W)	*N*†	Apparent ages		Isochron analysis		
					Weighted mean age (ka ± 2σ)§	MSWD	$^{40}Ar/^{36}Ar_i$ (±2σ)	Age (ka ± 2σ)	MSWD
Old Cone									
DBF-03-11	ocl1/da	18°13.286′	69°15.620′	21 of 23	***52.3 ± 2.8***	1.04	348.5 ± 56.4	45.3 ± 6.9	0.84
Dome Plateau									
PAR-03-23	du/dat	18°10.421′	69°10.897′	25 of 29	***41.8 ± 3.6***	2.80	297.2 ± 6.7	41.5 ± 3.0	1.66
PAR-03-04	du/dat	18°11.134′	69°10.368′	24 of 25	***41.8 ± 2.4***	1.40	295.4 ± 2.4	41.8 ± 3.2	1.23
PAR-03-18	d2	18°12.220′	69°09.642′	30 of 33	***43.6 ± 2.4***	1.70	294.5 ± 3.0	45.1 ± 3.2	1.34
DBF-03-08	du/da	18°13.292′	69°15.466′	22 of 28	46.6 ± 2.9	1.67	314.3 ± 10.7	***44.0 ± 2.3***	1.02
DBF-03-02	du/da	18°12.950′	69°13.569′	15 of 21	***45.9 ± 1.5***	1.00	295.2 ± 7.4	45.9 ± 2.0	0.98

Note: MSWD—mean square of weighted deviations.
*Samples collected from the debris avalanche are noted xxx/da or xxx/dat, where xxx is the chemically correlated unit and da indicates debris avalanche and dat indicates Toreva block.
†Total number of incremental-heating steps + total fusion steps included in statistics reported in following columns.
§Ages were calculated relative to 1.194 Ma Alder Creek Rhyolite sanidine (Renne et al., 1998); uncertainties are reported at 2σ precision.

preferential incorporation of xenocrystic biotite from crustal wall rocks shortly before eruption, such that any accumulated radiogenic argon was not completely degassed, similar to the situation reported in plagioclase at Tatara–San Pedro (Singer et al., 1998) and biotite at Nevado de Toluca, Mexico (Arce et al., 2006). Alternatively, juvenile biotite may contain excess argon in its structure (e.g., Phillips and Onstott, 1988). We intend to more fully pursue the origin of the anomalously old biotite in the Dome Plateau lavas in a separate paper.

For Dome Plateau samples not moved by the debris avalanche, textural heterogeneity between outcrops masks uniformity in age and chemistry, and therefore, data from samples of similar age and chemistry were combined, defining units d2 and d3, each of which represents a chemically and temporally distinct flow unit. For completeness, data from individual samples within a flow unit are reported separately in Tables 2–4, but they are pooled to yield a more precise age in Figure 5A, which gives the best age for these units.

A small number of SCLF ages and one laser incremental-heating age from sanidine in the Dome Plateau lavas are older than the bulk of the data; this, for some samples, resulted in skewed cumulative probability distributions or multiple peaks of elevated age probability (e.g., Fig. 5A). This is similar to findings by Ton-That et al. (2001) and Smith et al. (2003) for distal ash beds contaminated by older xenocrysts. Like those and many other studies, we infer that the most reasonable age corresponds with the youngest of the local probability maxima, and we interpret skewness and older peaks to reflect a small number of xenocrysts that were not completely degassed at the time of eruption. For example, in Figure 5A, two of eighteen separate sanidine ages are excluded from the weighted mean age calculation, resulting in an acceptable mean square of weighted deviates (MSWD) value and an age of 44.6 ± 1.7 ka for the d2 dome.

ERUPTIVE CHRONOLOGY

The 17 volcanic units shown in Figure 3 are arranged into six groups, based on age,

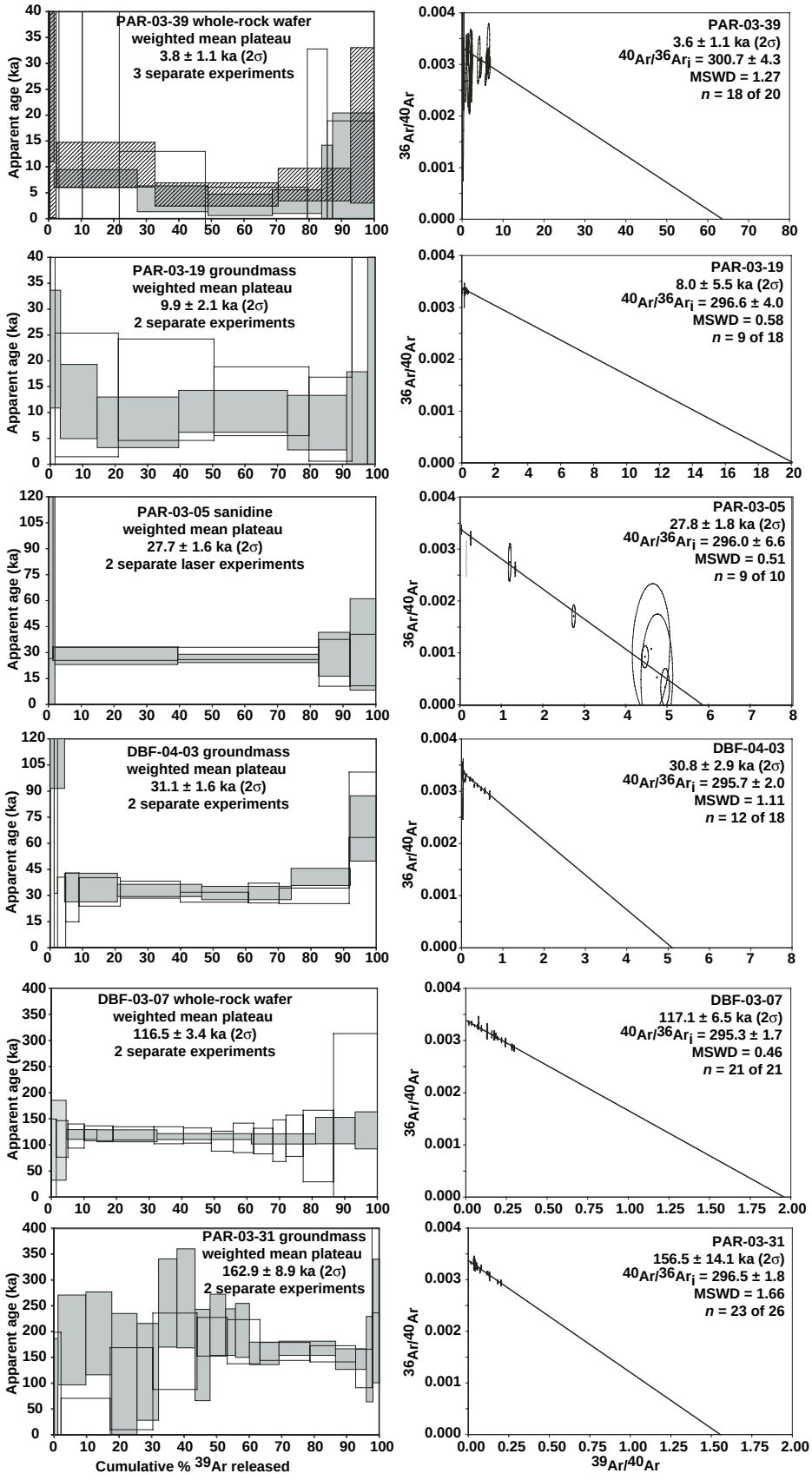

Figure 4. Age spectra and inverse isochron diagrams for representative Parinacota samples, exemplifying the utility of step heating in detecting effects of Ar-loss, excess Ar, and phase inhomogeneity. PAR-03-39 (ycl whole-rock wafer) has saddle-shaped age spectra, and the inverse isochron $^{40}Ar/^{36}Ar$ intercept does not overlap the atmospheric value, indicative of small amounts of excess Ar. In contrast PAR-03-19 (ycl groundmass) has relatively flat age spectra and atmospheric $^{40}Ar/^{36}Ar$ intercept. PAR-03-05 (ocb sanidine) has high radiogenic yield corresponding to precise step ages. DBF-04-03 is a prismatically jointed block from the debris avalanche. Increasing age with heating temperature is indicative of undegassed, refractive xenocrysts. DBF-03-07 is an aphyric whole-rock sample of Chungará andesite. PAR-03-31 (ca) likely experienced some Ar-loss (younger ages from low-temperature heating steps, especially in the unshaded experiment). MSWD—mean square of weighted deviations.

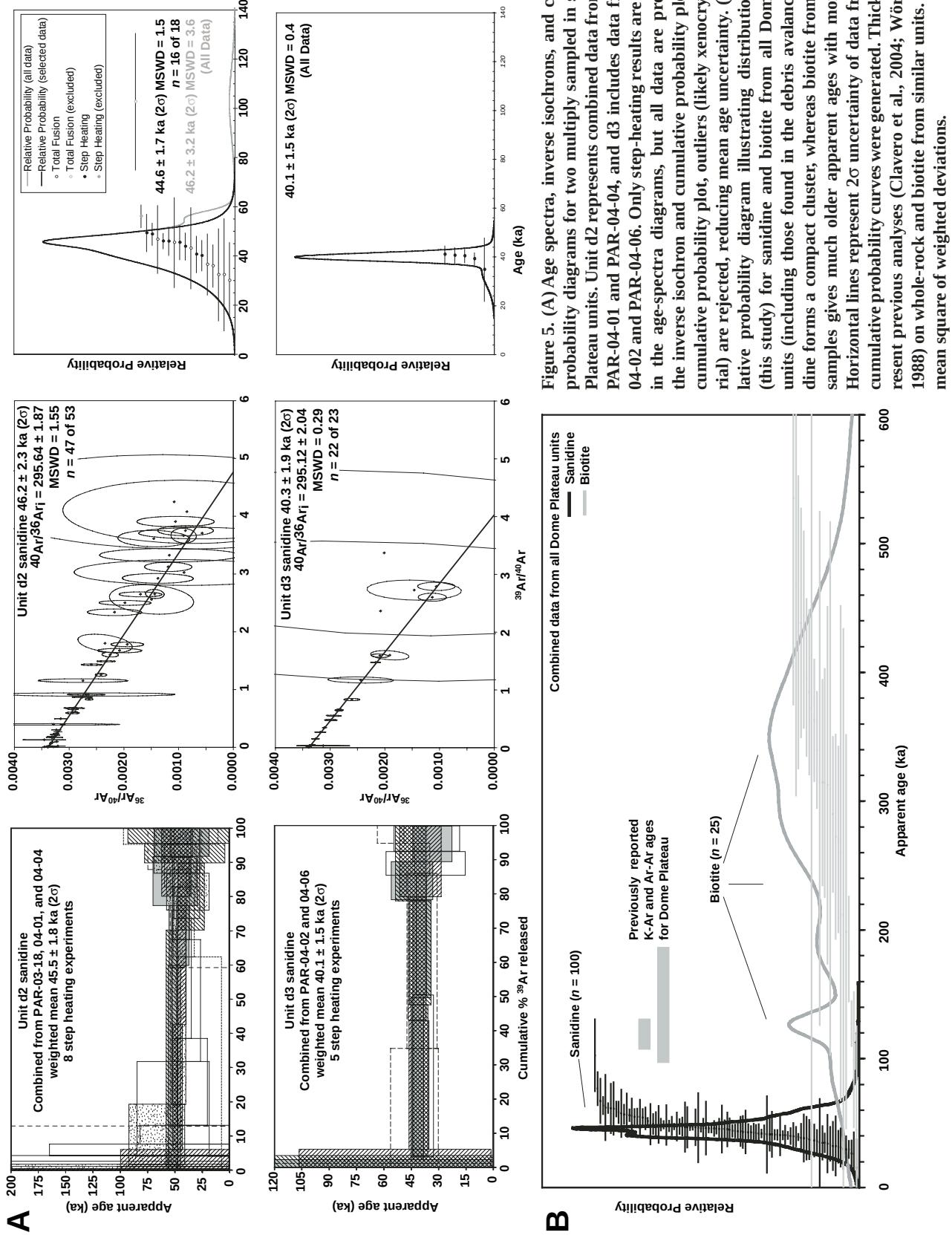

Figure 5. (A) Age spectra, inverse isochrons, and cumulative probability diagrams for two multiply sampled in situ Dome Plateau units. Unit d2 represents combined data from samples PAR-04-01 and PAR-04-04, and d3 includes data from PAR-04-02 and PAR-04-06. Only step-heating results are presented in the age-spectra diagrams, but all data are presented in the inverse isochron and cumulative probability plots. In the cumulative probability plot, outliers (likely xenocrystic material) are rejected, reducing mean age uncertainty. (B) Cumulative probability diagram illustrating distribution of ages (this study) for sanidine and biotite from all Dome Plateau units (including those found in the debris avalanche). Sanidine forms a compact cluster, whereas biotite from the same samples gives much older apparent ages with more scatter. Horizontal lines represent 2σ uncertainty of data from which cumulative probability curves were generated. Thick bars represent previous analyses (Clavero et al., 2004; Wörner et al., 1988) on whole-rock and biotite from similar units. MSWD—mean square of weighted deviations.

TABLE 5. REPRESENTATIVE WHOLE-ROCK MAJOR-ELEMENT COMPOSITIONS OF PARINACOTA LAVAS

Unit:	Chungará andesites		Dome Plateau		Old Cone			Border Dacite	Young Cone		Ajata flows			
Map symbol:	(ca)		(d2)	(d3)	(ocl1)	(ocl2)	(oclb)	(ocb)	(ycl)		(a1)	(a2)	(a3)	(a4)
	PAR	PAR	PAR	PAR	PAR	PAR	PAR	PAR	PAR	PAR	PAR	PAR	PAR	PAR
Sample no.:	03-31	03-22	04-01	04-02	03-10	03-28	03-36	03-05	03-14	03-15	03-20	219	222	03-25
(wt%)														
SiO_2	57.30	59.50	67.30	68.50	62.20	59.90	61.70	63.80	59.10	57.50	58.50	56.66	53.32	58.70
TiO_2	1.31	1.15	0.50	0.53	0.94	1.17	1.11	0.82	1.33	1.35	1.27	1.40	1.63	1.26
Al_2O_3	15.90	16.00	14.50	14.60	15.50	15.70	15.40	16.00	16.10	16.40	16.20	16.46	15.90	16.40
Fe_2O_3tot	6.94	6.11	2.94	3.10	5.14	6.14	5.41	4.21	6.79	7.10	6.82	8.39	8.69	6.77
MnO	0.09	0.08	0.05	0.05	0.07	0.08	0.07	0.06	0.09	0.09	0.09	0.11	0.11	0.09
MgO	3.44	2.90	1.01	1.10	2.30	3.06	2.26	1.77	3.21	3.23	3.20	4.15	5.03	3.18
CaO	5.77	5.13	2.23	2.37	4.22	5.20	4.29	3.77	5.51	5.68	5.46	6.56	7.52	5.47
Na_2O	4.11	4.11	4.02	4.14	4.24	4.32	4.43	4.49	4.28	4.30	4.28	4.14	4.28	4.30
K_2O	3.00	3.18	4.09	4.18	3.51	3.10	3.41	3.48	2.90	2.87	2.86	2.27	2.49	2.86
P_2O_5	0.50	0.43	0.18	0.18	0.35	0.44	0.44	0.32	0.48	0.49	0.46	0.42	0.77	0.46
Total	98.36	98.58	96.82	98.75	98.47	99.10	98.51	98.72	99.79	99.00	99.13	100.56	99.73	99.48

Note: X-ray fluorescence (XRF) data are from University of Göttingen, using methods of Hinners et al. (1998).

chemistry, and texture, although portions of some groups are coeval (i.e., the age ranges of Young Cone and Ajata flows, and Old Cone and Dome Plateau, respectively, overlap significantly). In no case does $^{40}Ar/^{39}Ar$ geochronology violate superposition. Representative chemical analyses are listed in Table 5, and a complete data set for all dated samples is presented in Table DR3 (see footnote 1).

Chungará Andesites (163–117 ka)

The oldest units preserved at the base of the Parinacota edifice are the Chungará andesites (ca). These lavas crop out as a low (>50-m-thick) shelf that forms the north shore of present-day Lago Chungará (Fig. 6A). Flow fronts are well preserved, indicating a southward flow direction, although the distance to the vent is unclear because it is beneath present-day volcanic edifices. There are multiple flow lobes, four of which have been dated; however, unambiguous mapping of contacts is precluded because most of the ca unit is covered by a veneer of recent pyroclastic material. The fifth and youngest sample from this group (116.5 ± 3.4 ka) was from a hummock in the debris avalanche composed entirely of ca, indicating that (1) Chungará andesites extend at least as far north as the inside of the collapse scarp, and (2) the plane of the detachment was deep enough in the volcano to sample ca material.

Chungará andesites have a relatively restricted range in composition, 57.3%–59.5% SiO_2 (Fig. 2). Following eruption of the Chungará andesites, there was a hiatus lasting 64.2 ± 6.2 k.y., which was previously unrecognized due to imprecise whole-rock and K-Ar and $^{40}Ar/^{39}Ar$ ages as old as 138.9 ± 42.8 ka (Clavero et al., 2004) from overlying units, as discussed already.

The age range of Chungará andesites falls into the period of cone building of nearby Pomerape Volcano, which occurred between 192 ± 12 ka and 106 ± 14 ka (based on whole-rock K-Ar dates of Wörner et al., 1988). Chucullu-Vilacollo andesite and Caquena domes represent two still older centers in the vicinity (275 ± 44 ka and 285 ± 53 ka; Wörner et al., 1988).

Rhyodacite Dome Plateau (47–40 ka)

Atop the Chungará andesites is a sequence of partially overlapping rhyodacite domes (66.6–68.6% SiO_2). These lavas were viscous and crystal-rich, resulting in dome heights of ~200 m, mostly located along the south and west flanks of the modern cone (Figs. 3, 6A, and 6D). Also present as hummocks and as intact Toreva blocks (Figs. 6B and 6D), Dome Plateau material was extensively moved by the later edifice collapse. This indicates that the original area occupied by the dome field extended from the southern base of the cone to beneath what is now the west flank of the modern cone, and that Toreva blocks likely moved only 1–2 km during the sector collapse. In addition, typical prismatically jointed blocks from block-and-ash-flow deposits of the same age and composition exist along the southern edge of the debris avalanche, suggesting that explosive activity was associated with these domes and that this material was subsequently moved by the debris avalanche. Dome Plateau lavas are rich in phenocrysts of plagioclase, pyroxene, sanidine, quartz, biotite, amphibole, sphene, and zircon, but lack olivine, making them among the most evolved and mineralogically diverse units on the volcano (Fig. 2).

Dome Plateau lavas remaining in situ are divided into four units, three of which have been dated. Unit d1 is a relatively small-volume dome, circular in map view, dated at 47.0 ± 1.3 ka. Unit d2 forms the most prominent plateau-forming mass, and it was sampled at three locations (PAR-03-18, PAR-04-01, and PAR-04-04). Pooled ages from these samples yield an age of 44.6 ± 1.7 ka (Fig. 5A). Dome d3 is southeast of d2 and has been sampled at two

Figure 6. Various views from the map area of Figure 3, indicating key stratigraphic relations and locations of dated samples from this study. Map units are described in Figure 3. (A) South side of Volcán Parinacota, photographed from near the south shore of Lago Chungará. Volcán Pomerape is the snow-covered peak behind Parinacota. (B) Detail of multiply sampled Toreva block, which records the contact between Dome Plateau (PAR-03-04) and two separate overlying Old Cone flows (PAR-03-02 and PAR-03-03). View is to the south, Parinacota is out of the field of view to the left. Dip of the contacts is toward the edifice, indicating block rotation. (C) View to the south from ~5200 m elevation on the south flank of Volcán Parinacota, down the valley between two ocb lava flows. Curved moraines are indicated in dashed lines. The eastern shore of Lago Chungará is in the extreme right background. (D) Proximal portion of the Parinacota debris avalanche; photo is from a location ~12 km from the summit. Prominent Toreva blocks up to 250 m high (dat) are indicated.

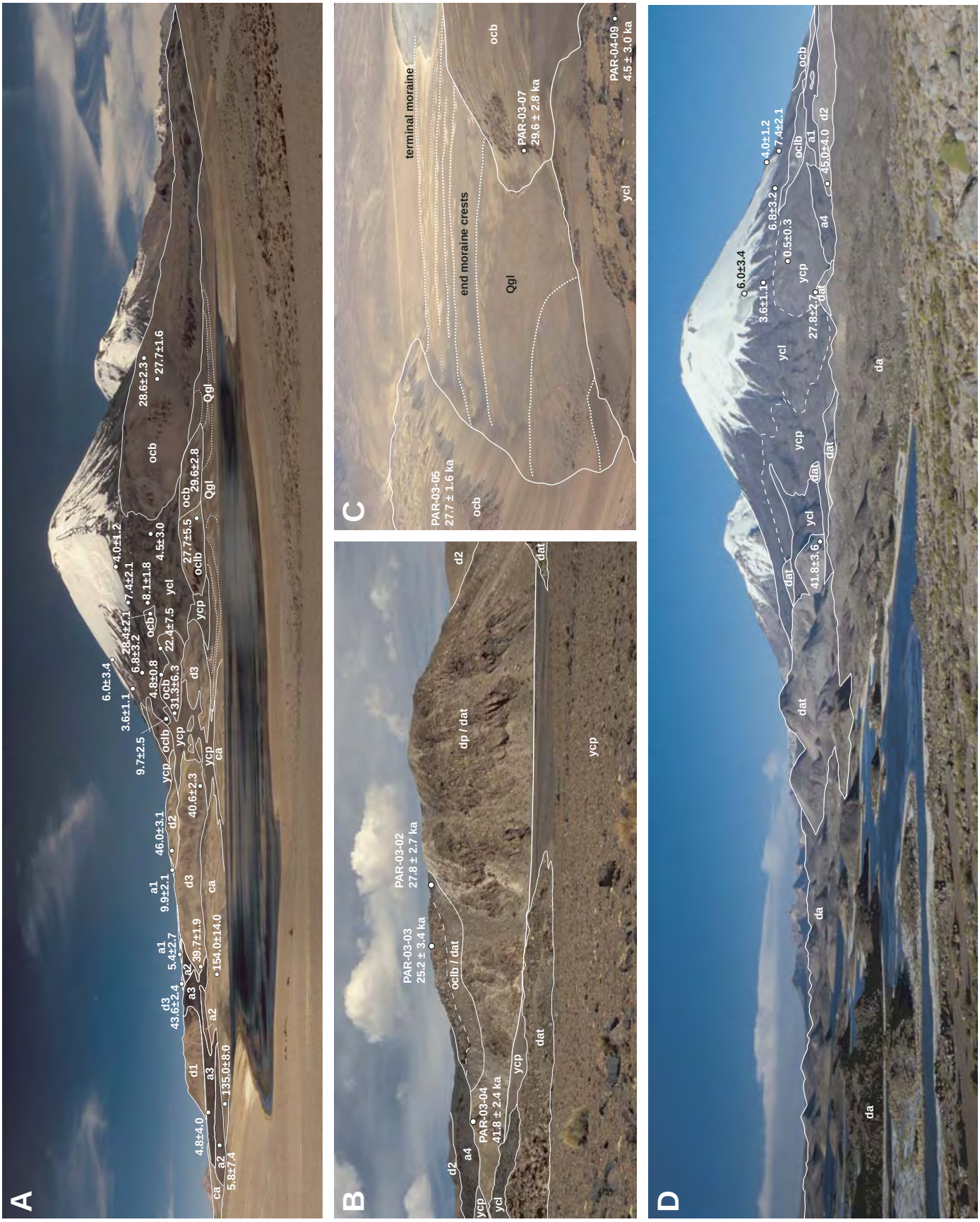
A
6.0±3.4
3.6±1.1
9.7±2.5
28.4±2.1
7.4±2.1
6.8±3.2
8.1±1.8
4.0±1.2
4.5±3.0
28.6±2.3
27.7±1.6
ocb
ycl
oclb
ycp
d2
d3
a1
a2
a3
a4
ca
d1
dat
Qgl
4.8±0.8
31.3±6.3
22.1±7.5
27.7±5.5
29.6±2.8
46.0±3.1
40.6±2.3
9.9±2.1
5.4±2.7
39.7±1.9
154.0±14.0
43.6±2.4
135.0±8.0
4.8±4.0
5.8±7.4
B
PAR-03-02
27.8 ± 2.7 ka
PAR-03-03
25.2 ± 3.4 ka
PAR-03-04
41.8 ± 2.4 ka
dp / dat
oclb / dat
d2
ycp
dat
C
terminal moraine
end moraine crests
PAR-03-05
27.7 ± 1.6 ka
PAR-03-07
29.6 ± 2.8 ka
PAR-04-09
4.5 ± 3.0 ka
ocb
Qgl
ycl
D
6.0±3.4
3.6±1.1
4.0±1.2
7.4±2.1
6.8±3.2
0.5±0.3
27.8±2.7
41.8±3.6
45.0±4.0
ycl
ycp
oclb
a1
a4
d2
dat
da

locations (PAR-04-02 and PAR-04-06), yielding a combined age of 40.1 ± 1.5 ka (Fig. 5A). Dome Plateau material was sampled at various locations within the debris avalanche, yielding ages of 45.9 ± 1.5, 45.3 ± 5.8, 44.0 ± 2.3, 41.8 ± 2.4, and 41.8 ± 3.6 ka, and whereas chemistry and texture is very similar to in situ units, unambiguous assignment cannot be made. A younger pulse of more silicic (Fig. 2) Dome Plateau–like material (based on chemistry and petrography and present only in the debris avalanche) erupted at 29.4 ± 6.1 ka (Table 3).

Old Cone (52–20 ka)

During approximately the same period that rhyodacite domes were extruded on the south and west sides of the volcanic center, less silicic dacitic magmas (62.2–64.3% SiO_2) (ocl1) were erupting on the northwest sides of the complex. One in situ outcrop has been dated at 46.7 ± 1.6 ka. Other examples are known from the debris avalanche (i.e., must have been sourced somewhere on the western side of the complex), and they span an age range from 52.3 ± 2.8 ka to 39.0 ± 3.0 ka (Table 2).

As building of the Old Cone continued (ocl2) in the interval 37.8 ± 6.8 to 20.0 ± 4.0 ka, compositions generally become more mafic (61.8–57.9% SiO_2). Lavas have a wide variety of textures, including some with large feldspar phenocrysts; however, all contain amphibole phenocrysts. Outcrops can be found on the northwest side of the complex, valley bottoms on the south flank, and a preserved portion of one flow to the south of the High Ajata flow, adjacent to dome d2. In situ lavas of ocl2 >60% SiO_2 only occur on the southwest side of the complex, whereas more mafic ocl2 lavas occur on the northwest slopes, adjacent to ocl1, as well as in the debris avalanche, indicating that they were common in the west and northwest portions of the Old Cone.

During the time ocl2 was being erupted, there was a brief episode of voluminous effusive activity, with formation of large coulees, which form the present border between Chile and Bolivia, called the Border Dacite by Wörner et al. (1988) (ocb on map, this study, and Fig. 6A). The two flow units, which are indistinguishable in age (28.0 ± 1.0 ka) based on numerous dated samples, together comprise the most voluminous single lava effusion on the volcano, forming a ridge 150–250 m high, 4 km long, and 2 km wide. The vent locations were likely beneath two dome-shaped features at 5250 m elevation on the southeast flank of the Old Cone. The lavas that make up the two flow lobes of the Border Dacite have 63.8 and 64.4% SiO_2, are phenocryst-rich, and have conspicuous feldspar megacrysts up to 2 cm in length.

Two kilometers west of these two flow lobes is another flow of similar height and length, but only ~1 km in width, and it has similar major-element chemistry and age (multiple samples analyzed ranging from 63.1% to 63.9% SiO_2). This western flow, also mapped as ocb, even though it is ~2–3 km from the border and entirely within Chile, is less conspicuous in outcrop since it is largely draped and concealed by younger, postavalanche pyroclastic flows from the Young Cone. The vent of the western flow likewise has been overrun by later Young Cone flows (Fig. 6A).

Together, the three flows that make up ocb unit represent ~3 km^3 of erupted magma, or ~7% of the total system output. The rapid succession of these large eruptions (i.e., indistinguishable age) and relative uniformity in chemistry indicate that a magma reservoir of at least that volume existed during this portion of the volcano's history. Also within this time span, a group of magmas intermediate in composition between ocl2 and ocb erupted from vents on the southwest flank, and are shown as oclb on Figures 3 and 6A. This eruptive phase (Dome Plateau and Old Cone) thus represents an increasingly focused reservoir compared to the times when Chungará andesites were erupted.

Glaciation (<28 ka)

Extent of glaciation on Central Andean volcanoes is modulated by regional climate (Thompson et al., 1998), amount of precipitation (Ammann et al., 2001), and by local edifice height. Similarly, edifice height is a function of both addition of material by eruptions and removal of material by glacial erosion. The period immediately following Border Dacite extrusion was characterized both by rapid edifice growth and by climatic conditions favoring glacial advance, as evidenced by low $\delta^{18}O$ values in ice cores from neighboring Sajama Volcano (Thompson et al., 1998). Glacial features such as striations and glacial erosion have been observed at the contact between Old Cone and Young Cone lavas, suggesting that the Old Cone was strongly affected by glaciation prior to collapse. In a valley between two ocb flows (Fig. 3), we recognized at least six arcuate moraine ridges 5–10 m high confined to the intraflow valleys (Fig. 6C). Thus, the ice cap on ancestral Parinacota must have reached its maximum extent after the ocb lavas were emplaced at 28 ka, and it was already retreating before the time of the debris avalanche, which would have abruptly removed the glacier accumulation zone and precluded the formation of nested moraines, features which are characteristic of a slow, not catastrophic glacial retreat.

This is consistent with recent determinations of local Last Glacial Maximum (LLGM) in the tropical Andes by ^{10}Be dating of nested moraine sequences, which indicate a LLGM around 28 ka with recessional moraines at 16.3 and 14.5 ka in valleys to the east of Lake Titicaca (Smith et al., 2005), and it is broadly consistent with the timing of the global LGM in the southern Andes and the Northern Hemisphere between 23 and 16 ka (Kaplan et al., 2004). The Sajama ice core (Thompson et al., 1998) reveals a long period of accumulation ending at 22 ka, followed by pulses of accumulation at 18 ka and 15 ka. Since at present the moraines on Parinacota are undated, any of the above events may be correlative to the precollapse glacial retreat at Parinacota.

Debris Avalanche (Between 20 and 10 ka)

The Parinacota debris avalanche removed a large portion of the edifice, consisting of rhyodacite domes and Old Cone lavas built up since 53 ka, depositing ~6 km^3 of debris across a 140 km^2 area of the Lauca valley to the west of Parinacota (Clavero et al., 2002). Proximally, the debris avalanche consists of slightly rotated Toreva blocks up to 250 m high with individual volumes approaching 0.05 km^3, which preserve internal stratigraphy. Indeed, one such block preserves the contact between Dome Plateau and ocl2 lavas (Fig. 6C). The main portion of the avalanche consists of hummocks that decrease in size in the distal direction (Fig. 6D). Since no syncollapse deposit of juvenile magmatic material has been found, it is likely that the collapse was not accompanied by a major eruption. While contemporaneous culmination of glacial retreat and volcanic sector collapse does not necessarily imply causality, the rapid retreat of glacial ice beginning ca. 16 ka might have caused significant changes in the hydrologic system of the volcano, which could have been a contributing factor to edifice failure around that time.

The upper limit on the age of the avalanche, as quantified by $^{40}Ar/^{39}Ar$, is the youngest andesite of the Old Cone (ocl2), dated at 20.0 ± 4.0 ka, which is cut by the avalanche. However, evidence presented in the preceding section implies that the Old Cone likely persisted until LGM time. The lower limit on the avalanche age is the oldest postcollapse lava, a flank Ajata vent eruption dated at 9.9 ± 2.1 ka. It is important to note, however, that all the Young Cone samples dated younger than 8.1 ± 1.8 ka are from the *surface* of the modern cone, which lacks significant incision by erosion. Therefore, the oldest Young Cone lavas are most likely older than the oldest *dated* Ajata and Young Cone flows. As a result of not being able to access the earliest

Young Cone history, the lower limit on debris avalanche age is likely to be significantly older than 10 ka, but remains poorly constrained. The younger than 10 ka Young Cone age is at odds with the interpretation of Clavero et al. (2002), who obtained ^{14}C dates as young as 8700 ± 200 cal yr B.P. from preexisting paleosoil material incorporated into the debris avalanche. The older collapse age, however, is consistent with the 18.2 ± 0.7 ka ^{3}He-exposure age from a block exposed by the avalanche (Wörner et al., 2000a). The ^{14}C dates from organic material overlying the debris avalanche deposit at Cotacotani also give an older age for the collapse between >11 and >13 ka (Ammann et al., 2001; Baied and Wheeler, 1993; Francis and Wells, 1988), which is again confirmed by a recent study on drill cores from Lago Chungará (Moreno et al., 2006). Further evidence comes from the timing of glaciation: If the Old Cone was decapitated by the collapse before the end of the LGM, then the glaciers on the Old Cone would have lost their source area, the glaciers must have disappeared immediately, and no moraine formation would have resulted. We therefore conclude that the most likely age of the collapse event is older than 13 ka and younger than 20 ka.

Young Cone (>8 ka–Recent)

Following sector collapse, a new stratovolcano was built of lava flows (ycl) and pyroclastic deposits (ycp) that are significantly more mafic than preceding lavas (Fig. 2). Because the interior of the cone, and its earliest history, are inaccessible, our geochronology represents only the youngest flows that drape the cone. Eight Young Cone lavas range from 8.1 ± 1.8 to 0.5 ± 0.3 ka and vary in composition from 57.5% to 59.1% SiO_2. Three blocks and bombs (59.2–60.1% SiO_2), likely sourced from the summit vent and found among pyroclastic material, were determined to be 4.8 ± 0.8, 4.3 ± 2.6, and 3.6 ± 1.1 ka, indicating that pyroclastic activity was associated with many Young Cone eruptions. These ages are consistent with a ^{3}He-exposure age of Wörner et al. (2000b) on a recent Young Cone flow (1.6 ± 0.4 ka). The Young Cone lavas and pyroclastics were erupted from the central crater only and are petrographically monotonous. This suggests an increasingly focused magma reservoir with respect to spatial distribution of centers and compositions of erupted magmas.

Ajata Flows (10–3 ka)

Coeval with the youngest part of Young Cone growth are a series of flank vents on the south side of the volcano. These vents have produced small, monogenetic scoria cones and a'a flows up to 3 km long. The first set of vents to become active was located between 4950 and 5000 masl (a1), and it produced numerous flows and some ejecta (Fig. 3). One flow is 9.9 ± 2.1 ka, and a bomb associated with this unit (58.5% SiO_2) is 5.4 ± 2.7 ka in age; therefore, geochronology cannot resolve whether these vents were active simultaneously or sequentially. The major-element chemistry of this unit is similar to that of Young Cone lavas. Farther down the south flank of the volcano, atop the rhyodacite Dome Plateau at 4800 masl, a series of closely spaced vents produced two nearly superimposed lava flows (a2 and a3) both of which cascaded down the south edge of the Dome Plateau and onto the surface formed by Chungará andesites. The lower of these flows (a2 = Lower Ajata of Wörner et al., 1988) has a composition of 56.7% SiO_2, and a poorly constrained age of 5.8 ± 7.4 ka. The upper of these flows (a3 = Upper Ajata of Wörner et al., 1988) is the most mafic composition erupted at Parinacota (53.3% SiO_2), and its $^{40}Ar/^{39}Ar$ age is 4.8 ± 4.0 ka. The $^{40}Ar/^{39}Ar$ ages for a2 and a3 are in agreement with the ^{3}He exposure ages of 6.0 ± 0.6 and 3.0 ± 0.5 ka (Wörner et al., 2000b). The youngest of the Ajata flows (a4 = High Ajata of Wörner et al., 1988) erupted from a vent at 4900 masl and resulted in a 3-km-long flow down the southwest side of the edifice, just within the scarp formed by the debris avalanche (Fig. 3). The $^{40}Ar/^{39}Ar$ age determination of 2.6 ± 1.3 ka closely matches four separate ^{3}He ages for this flow, ranging from 1.3 to 2.2 ka (Wörner et al., 2000a). Like the other Ajata flow sourced at a high-elevation vent, its chemistry (58.7% SiO_2) is more similar to that of Young Cone lavas than to the significantly more mafic a2 and a3 Ajata flows, which erupted further downslope. Both $^{40}Ar/^{39}Ar$ dates and ^{3}He dates are in accord with the relative stratigraphy established on the basis of superposition, surface weathering, and lichen growth.

MAGMA COMPOSITION THROUGH TIME

Using the new $^{40}Ar/^{39}Ar$ chronology, we examined compositional trends as a function of time. Many lithologies found in the debris avalanche can be correlated to in situ counterparts, allowing time versus composition information to be extracted from debris avalanche samples where stratigraphic position has been compromised. Figure 7 places major-element compositions in a temporal framework.

The 65 k.y. hiatus between Chungará andesites and the rest of the Parinacota history raises

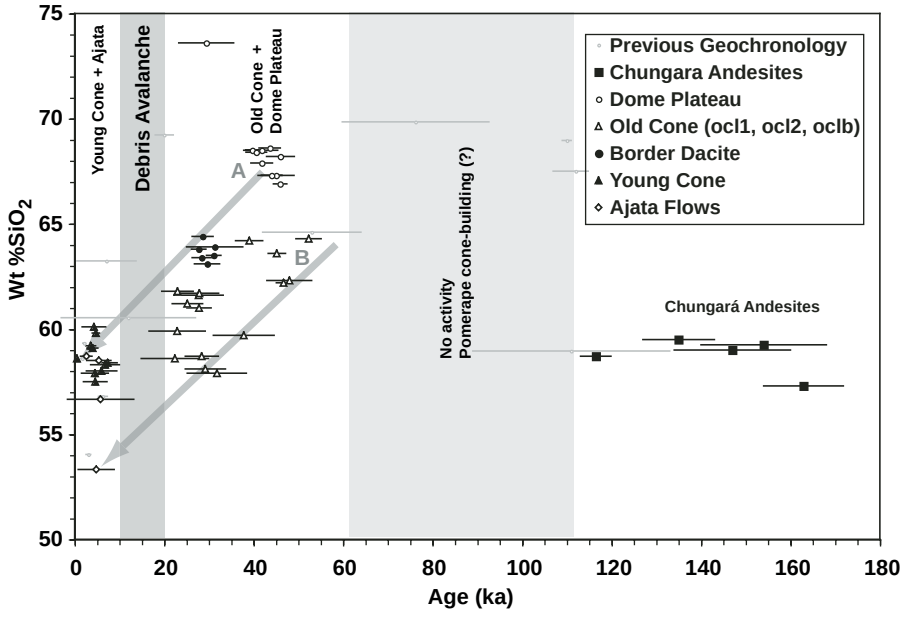

Figure 7. SiO_2 versus time plot for University of Wisconsin–dated samples (black) and previously reported K-Ar (Wörner et al., 1988), $^{40}Ar/^{39}Ar$ (Clavero et al., 2004), and ^{3}He exposure dates (Wörner et al., 2000a) (gray). Error bars reflect 2σ uncertainties in age. Vertical gray bands indicate periods where no lavas were sampled, due to either hiatus or shifting of magmatism during Pomerape cone building as well as the period after sector collapse when inception of Young Cone growth occurred. The area between vectors A and B represents mixing between Old Cone, Dome Plateau, and two end-member Ajata compositions.

the possibility that there may be no direct link between the two magmatic systems. In fact, Chungará andesites erupted at the same time as the main episode of Pomerape cone building and may be related to the older, spatially distributed phase of volcanic activity in the area. The greatest variability in erupted compositions occurred during the Old Cone–Dome Plateau period of the volcano's history. In the time period between 40 and 50 ka, the persistence of a group of magmas <65% SiO_2, during the time that Dome Plateau eruptions >67% SiO_2 were also occurring, indicates a compartmentalized magmatic system, with one portion feeding the andesitic to dacitic ocl1 lava flows and the other portion feeding the rhyodacitic dp eruptions. It is thus likely that during the earlier period (Chungará andesites, Pomerape, Dome Plateau, and early Old Cone), magmas ascended and evolved in parts of the shallow plumbing system that were unconnected or at least well separated.

This situation changed significantly during the subsequent evolution of Parinacota. During the course of the Old Cone construction, a broad trend toward more mafic compositions is seen, as well as a trend toward increased variability of erupted compositions (Fig. 7). Also within this time period, voluminous Border Dacite, and Old Cone rocks as mafic as 57.9% SiO_2 erupted. This corroborates the hypothesized persistence of end-member compositions during intratrend mixing identified by Davidson et al. (1990). Young Cone compositions are on average much less variable, more mafic, and approach those of the Ajata flows. This is consistent with observations that the two Ajata components, corresponding to the compositions of the a2 and a3 flows, were mixing end members (Fig. 7) and that both had persistently recharged the system long before their actual eruption (Davidson et al., 1990; Ginibre et al., 2002b; Wörner et al., 1988).

Except for the low-volume Ajata flows, all eruptions subsequent to sector collapse were sourced at the summit crater. It appears that the systematic variation in compositional variability and location of eruptive centers is linked to a continuous evolution of the subvolcanic plumbing system, which became more focused, and erupted magmas became more mafic with time. The cataclysmic sector collapse only accelerated the tendency toward more mafic eruptions, posing the question of a feedback between this catastrophic unloading of the edifice and events in the subvolcanic plumbing system. The evolution of Volcán Parinacota can be viewed in the context of modeling by Pinel and Jaupart (2000, 2004a, 2004b), who described an interrelationship between volcanic edifice growth and the composition of magmas that are able to reach the surface. By loading Earth's surface, a volcano alters the stress field at depth, acting to prevent higher-density magmas from erupting. With time, the growing edifice acts as a compositional filter that allows only increasingly differentiated (i.e., lower density) magmas to reach the surface (Pinel and Jaupart, 2000). The chemical trends at Volcán Parinacota suggest that Ajata-type magmas were present in the subvolcanic magma system prior to collapse as mixing end members, and in light of these arguments, their eruption may have been impeded by the presence of the Old Cone edifice itself. Removal of the edifice by collapse may have allowed the less-differentiated magmas to erupt (Pinel and Jaupart, 2000). Edifice destruction has also been modeled to increase shallow reservoir replenishment with magma from depth (Pinel and Jaupart, 2005), resulting in increased flux and rapid rebuilding of collapsed volcanoes, as described in the following section.

VOLUME EVOLUTION OF THE VOLCANIC COMPLEX

Volumes for each erupted unit were calculated (methods are given in the GSA Data Repository, see footnote 1) and are presented in Table 6, and they are graphically depicted in Figure 8. Despite being areally extensive, the Chungará andesites are relatively thin and thus represent only ~6 ± 2 km^3 of material, or ~13% of the total volume. During this period of Parinacota's history (163–117 ka), effusion rates were low, with a mean rate of 0.13 km^3/k.y. This phase of relatively low eruptive rates coincided with spatially distributed volcanic activity in the area, which suggests that a focused magma reservoir had not yet developed at this early stage in the evolution of the complex. As initiation of Old Cone growth began on the north side of the complex, Dome Plateau extrusion occurred to the south, and eruption rates began to increase. Until ca. 35 ka, Parinacota's morphology was likely a complex of intermediate to silicic domes. Since many of the ocl1 and ocl2 samples were collected in the debris avalanche, only an average rate (0.46 ± 0.11 km^3/k.y.) can be calculated for this interval. Superimposed on this background were two periods of elevated activity during the building of the Dome Plateau (an additional 0.50 ± 0.18 km^3/k.y. for 6 k.y.) and Border Dacite (likely a single, short-lived pulse of 3.0 km^3 of magma).

After the debris avalanche, magma flux through the system increased, and ~14.9 ± 3.6 km^3 of magma was erupted between the time of the debris avalanche and the present day. The oldest Young Cone sample dated is 8.1 ± 1.8 ka, and using this as the constraint for initiation of Young Cone–building results in an eruption rate of ~2 km^3/k.y. However, these samples are from the outer surface of the cone, and the oldest interior of the cone is inaccessible. Assuming that the onset of Young Cone growth began at 15 ka, calculations of eruption rates give ~1.0 km^3/k.y. If instead, the debris avalanche occurred shortly after the last dated Old Cone sample (20 ka), and onset of Young Cone building was immediately afterward, then a minimum flux rate is only 0.75 km^3/k.y. An increase in abundance of black ash layers in drill cores from sediments of Lago Chungará around 7 ka (Moreno et al., 2006) suggests that the oldest Young Cone activity was mostly lava flows, and any small ash plumes did not reach high enough to overcome the barrier left by the collapse scar on the Old Cone. This is consistent with scoria flows on the surface of the Young Cone and black wind-blown ash covering the lower slopes of the volcano and adjacent plains.

The new $^{40}Ar/^{39}Ar$ ages, in particular the younger ages on the Dome Plateau and recognition of a 65 k.y. eruptive hiatus, result in a more condensed history of cone building, and result in effusion rates for the Old Cone part of the history ~3× higher than those based on the K-Ar age of 112 ka (Wörner et al., 1988). In comparison to

Figure 8. Time line of events at Volcán Parinacota over the past 163 k.y., also depicted in the series of panoramic photos of Volcán Parinacota taken from the south. Black portions of the time line indicate no eruptions. Colored squares each represent 1 km^3 of erupted magma. Cumulative erupted volume versus age plot of Parinacota compared with other arc volcanoes for which flux data exist is shown at lower right. To facilitate comparison, all volcanoes are plotted only for the past 200 yr; therefore, longer-lived systems are set to zero at 200 ka (for those cases, indicated final erupted volume is not accurate, as eruptions prior to 200 ka are not included in the total). Red-shaded region for Parinacota represents the region spanned by conservative and liberal estimates of erupted volume for each stage. Uncertainty envelope contracts at younger ages, since estimates of Old and Young Cone volumes are not independent of one another. A maximum Old Cone estimate necessitates a minimum Young Cone estimate and vice versa.

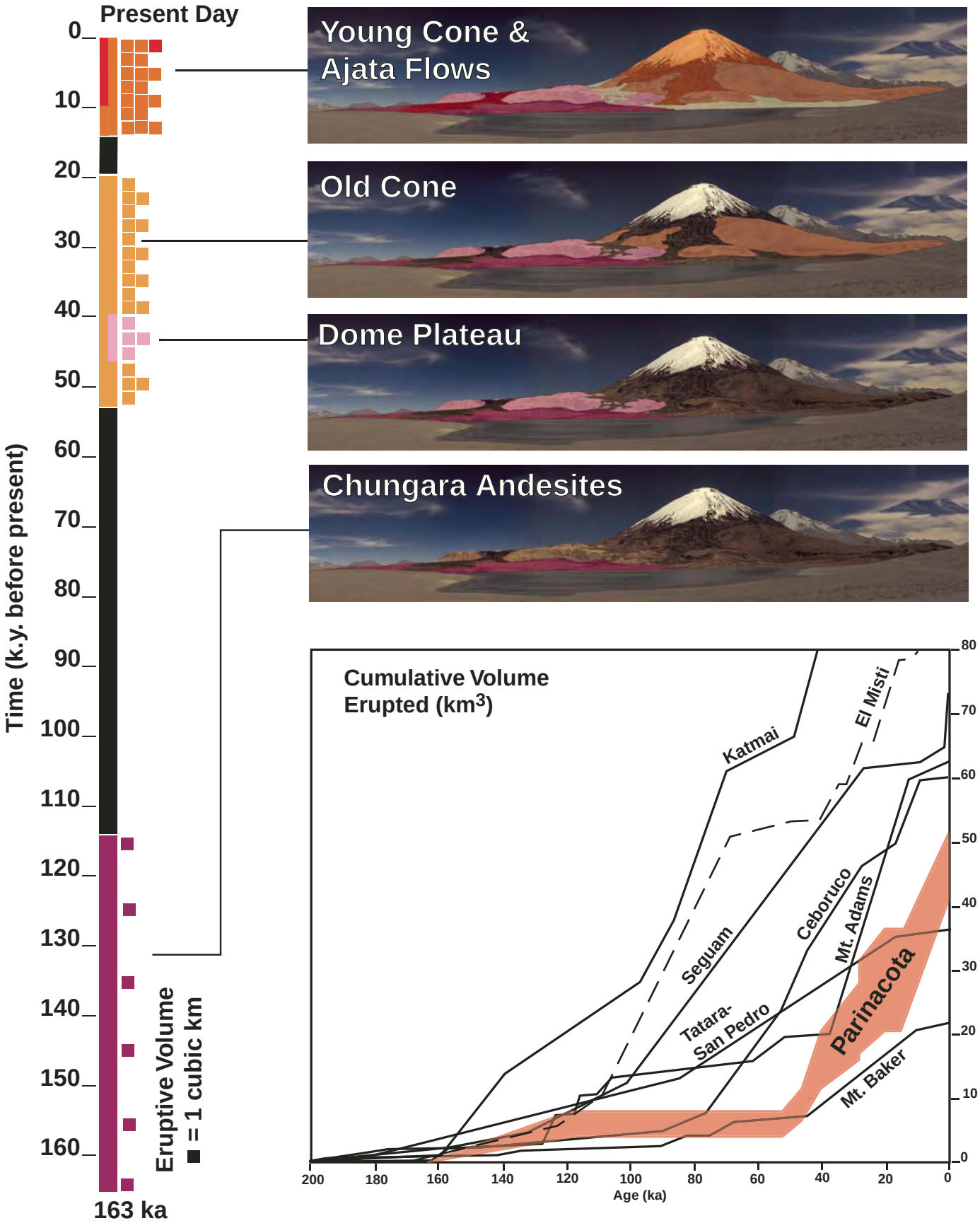
Present Day
0
10
20
30
40
50
60
70
80
90
100
110
120
130
140
150
160
163 ka
Time (k.y. before present)
Eruptive Volume
■ = 1 cubic km
Young Cone &
Ajata Flows
Old Cone
Dome Plateau
Chungara Andesites
Cumulative Volume
Erupted (km3)
Katmai
El Misti
Seguam
Ceboruco
Mt. Adams
Tatara-
San Pedro
Parinacota
Mt. Baker
200
180
160
140
120
100
80
60
40
20
0
Age (ka)
80
70
60
50
40
30
20
10
0

TABLE 6. ESTIMATED ERUPTED VOLUMES FOR PARINACOTA AND CORRESPONDING ERUPTIVE FLUXES

Unit description	Age	Min. volume (km^3)		Min. flux (km^3/k.y.)	Max. volume (km^3)		Max. flux (km^3/k.y.)
Ajata flows (a1, a2, a3, a4)	10–3 ka		0.1	0.01		0.2	0.03
Young Cone (ycl, ycp)*,†	ca. 5–0 ka		18.5	1.23		11.3	0.75
Old Cone							
Old Cone, in situ (ocl1, ocl2, oclw)	52–20 ka	11.0			18.3		
Border Dacite, in situ (ocb, oclb)	28 ka	2.5			3.5		
Old Cone, Border Dacite in debris avalanche (da)	52–20 ka	3.0			5.0		
Old Cone subtotal	52–20 ka	>>>	16.5	0.52	>>>	26.8	0.84
Dome Plateau							
Dome Plateau, in situ (d1, d2, d3)	47–40 ka	1.25			1.75		
Dome Plateau, in debris avalanche (da, dat)	47–40 ka	1.00			3.00		
Dome Plateau subtotal	47–40 ka	>>>	2.3	0.32	>>>	4.8	0.68
Chungará andesites (ca)	163–117 ka		4.0	0.09		8.0	0.17
Total volumes and average rates for all units			41.4	0.25		51.1	0.31

*For flux calculation, a more realistic Young Cone duration of 15 k.y. is used since 8 ka is the oldest age of the cone surface.

†The main source of uncertainty in Old and Young Cone volumes is the shape and depth of the debris avalanche scarp; therefore, maximum Old Cone volume necessitates a minimal Young Cone volume estimate, as described in the text.

the other arc volcanoes that have been studied in similar detail (Fig. 8), an average magmatic flux of 0.75 km^3/k.y. over both cone-building phases of Parinacota (past 52 k.y.), and the Young Cone flux of 1.0 km^3/k.y. (past 15 k.y.) is within the range (~0.2–5 km^3/k.y.) spanned by volcanoes on much thinner crust.

Wörner et al. (2000a) argued that two distinct end-member types of stratovolcanoes exist in the Central Volcanic Zone: (1) long-lived centers that have a variety of morphologies, characterized by low input/output rates and a variety of erupted compositions, and (2) rapidly built conical stratocones with smaller chemical variability. They speculated that crustal-scale fractures may act as a focusing mechanism that results in "fast" volcanic centers, whereas absence of such features impedes magma transit through the crust and results in development of lower-flux centers. Preliminary data indicate that the similarly sized and recently active Volcán Taapaca (~50 km west of Volcán Parinacota), which erupted relatively monotonous silicic andesite/dacite magmas, commenced its eruptions at 1.2 Ma, indicating an ~20× slower flux rate than at Parinacota, even though all subduction-related parameters are identical. On the other hand, El Misti Volcano in southern Peru, which has an average eruption rate of 0.63 km^3/k.y. (Thouret et al., 2001), is very similar to Parinacota's Young Cone phase

Faults have been implicated as ascent pathways for evolved magmas through the brittle upper crust (e.g., Petford et al., 2000). The Condoriri lineament, an extensional graben along which the Condoriri, Pomerape, and Parinacota volcanoes are located, may be such a magma-focusing feature. While the local stress configuration in the crust may explain the location of high-output volcanoes, it does not immediately explain the large variability in flux over time at Parinacota. Other factors, such as heating of wall rocks in the immediate vicinity of the conduit area and frequency of magmatic recharge, could act to modulate output through time

DISCUSSION

The $^{40}Ar/^{39}Ar$ ages of 57 lava samples from Parinacota range from 163 to 3 ka and provide a new chronostratigraphy that reveals time-dependent behavior of the magmatic plumbing system. Comprehensive geochronology used in concert with chemistry and mapping has revealed a more complete view of the evolution of the Parinacota volcanic complex through its variability in vent location, eruptive rate, and chemistry as a function of time. Sixteen analyses of Holocene Young Cone and Ajata flow samples have demonstrated that reliable $^{40}Ar/^{39}Ar$ ages can be produced for very young groundmass and whole-rock samples, extending the usable age range for this technique to 3–4 ka. Combined with volume estimates for the Young Cone, they demonstrate that magmatic flux has been increasing through the volcano's evolution along with a development of a spatially and compositionally more focused system. Clavero et al. (2002) reported on Indian legends that imply recent eruptions from Parinacota. This evidence and the young ages reported here suggest that the continuous evolution of the magma reservoir is still ongoing and that this system must be regarded as potentially active.

The new chronology elucidates new interrelationships among edifice morphology, volumes and compositions of magmas, and the behavior of the shallow magmatic system. Timing of eruptions allows us to reconstruct the succession of magmas that populated the magmatic system, which, in the Old Cone portion of the volcano's history, was more likely a coexistence than a succession. Coeval eruption of significantly different magma compositions from different vents suggests that the magmatic system was more laterally compartmentalized during the earlier stages of volcano evolution than previously thought. The Dome Plateau lavas (3.5 km^3) and Border Dacite (2.5 km^3) are largely homogeneous batches of magma with consistent textures and restricted compositional range, respectively, independent of the heterogeneity prevalent in the other Old Cone lavas of this time period. The trend toward mafic compositions and rapid rebuilding of the volcano following collapse suggest that the presence of a large edifice has an effect on the behavior of its underlying plumbing system and modulates the short-term flux from it.

Eruptive rates at Volcán Parinacota were highly variable. The presence of lacunae in the volcanic record, separating periods of intense magmatism accompanying cone growth, are similar to patterns seen in volcanoes in other arcs. During periods of cone building, surface flux at Parinacota was comparable to—and in some cases was higher than—that of volcanoes on thinner crust. A comparison of Parinacota and preliminary data from Taapaca supports the hypothesis that there is nothing intrinsic about thick crust that retards magma transit, but instead local crustal structure, locally variable recharge rates from the deep reservoir, and input from the mantle wedge are more significant variables. While rates of cone building and volumes of just the main cones are similar among Parinacota and volcanoes in other arcs, total volumes are smaller at Parinacota relative to the other well-studied volcanic areas in Figure 8. Many of those other studies include both the main cone and peripheral volcanism, but at Parinacota, and indeed in most of the Central Volcanic Zone, there is no peripheral volcanism. Whereas crustal thickness does not seem to have much of an effect on the building of large cones made of andesitic to rhyolitic composition, it does seem to affect the total eruptive flux by quashing the distributed basaltic component of arc volcanism in the Central Volcanic Zone.

ACKNOWLEDGMENTS

We sincerely thank Jorge Clavero at SERNAGEOMIN for sharing his mapping and extensive knowledge that facilitated work at Parinacota, and Xifan Zhang,

Lee Powell, and Brian Jicha for sharing their expertise, as well as helping to maintain the Rare Gas Geochronology Laboratory at University of Wisconsin–Madison. The outstanding staff at the OSU Radiation Center supplied a consistent stream of fast neutrons without a hitch. We are grateful to Carlos Nassar and CONAF for their hospitality and permission to work and sample in Parque Nacional Lauca. We would also like to thank Rebecca Lange and Terry Spell for their careful reviews and many thoughtful comments that helped us improve the paper. Our work was supported by U.S. National Science Foundation (NSF) grants EAR-0337667 and EAR-0516760 to Singer, Geological Society of America (GSA) Research, Sigma Xi, and Departmental Weeks Grants to Hora, and the Leibniz Award Wo362/18-1 of the German Science Foundation (DFG) to Wörner.

REFERENCES CITED

Addicott, W.O., Richards, P.W., and Sidlauskas, F.J., 1981, Plate-tectonic map of the circum-Pacific region: Tulsa, Oklahoma, American Association of Petroleum Geologists, scale 1:10,000,000.

Ammann, C., Jenny, B., Kammer, K., and Messerli, B., 2001, Late Quaternary glacier response to humidity changes in the arid Andes of Chile (18–29 degrees S): Palaeogeography, Palaeoclimatology, Palaeoecology, v. 172, no. 3–4, p. 313–326, doi: 10.1016/S0031-0182(01)00306-6.

Arce, J.L., Macias, J.L., Gardner, J.E., and Layer, P.W., 2006, A 2.5 ka history of dacitic magmatism at Nevado de Toluca, Mexico: Petrological, $^{40}Ar/^{39}Ar$ dating, and experimental constraints on petrogenesis: Journal of Petrology, v. 47, no. 3, p. 457–479, doi: 10.1093/petrology/egi082.

Baied, C.A., and Wheeler, J.C., 1993, Evolution of high Andean Puna ecosystems—Environment, climate, and culture change over the last 12,000 years in the central Andes: Mountain Research and Development, v. 13, no. 2, p. 145–156.

Bourdon, B., Wörner, G., and Zindler, A., 2000, U-series evidence for crustal involvement and magma residence times in the petrogenesis of Parinacota volcano, Chile: Contributions to Mineralogy and Petrology, v. 139, no. 4, p. 458–469, doi: 10.1007/s004100000150.

Clavero, J.E., 2002, Evolution of Parinacota Volcano and Taapaca volcanic complex, central Andes of northern Chile [Ph.D. thesis]: Bristol, University of Bristol, 248 p.

Clavero, J.E., Sparks, R.S.J., and Huppert, H.E., 2002, Geological constraints on the emplacement mechanism of the Parinacota debris avalanche, northern Chile: Bulletin of Volcanology, v. 64, no. 1, p. 40–54, doi: 10.1007/s00445-001-0183-0.

Clavero, J.E., Sparks, R.S.J., Polanco, E., and Pringle, M.S., 2004, Evolution of Parinacota volcano, central Andes, northern Chile: Revista Geologica de Chile, v. 31, no. 2, p. 317–347.

Coira, B., Davidson, J., Mpodozis, C., and Ramos, V., 1982, Tectonic and magmatic evolution of the Andes of northern Argentina and Chile: Earth-Science Reviews, v. 18, no. 3–4, p. 303–332, doi: 10.1016/0012-8252(82)90042-3.

Crisp, J.A., 1984, Rates of magma emplacement and volcanic output: Journal of Volcanology and Geothermal Research, v. 20, no. 3–4, p. 177–211, doi: 10.1016/0377-0273(84)90039-8.

Davidson, J.P., McMillan, N.J., Moorbath, S., Wörner, G., Harmon, R.S., and Lopez-Escobar, L., 1990, The Nevados de Payachata volcanic region (18°S, 69°W, N Chile): II. Evidence for widespread crustal involvement in Andean magmatism: Contributions to Mineralogy and Petrology, v. 105, no. 4, p. 412–432, doi: 10.1007/BF00286829.

Davidson, J.P., Hora, J.M., Garrison, J.M., and Dungan, M.A., 2005, Crustal forensics in arc magmas: Journal of Volcanology and Geothermal Research, v. 140, no. 1–3, p. 157–170, doi: 10.1016/j.jvolgeores.2004.07.019.

de Silva, S.L., and Francis, P., 1991, Volcanoes of the central Andes: Berlin, Springer-Verlag, 216 p.

Druitt, T.H., Edwards, L., Mellors, R.M., Pyle, D.M., Sparks, R.S.J., Lanphere, M., Davies, M., and Barriero, B., 1999, Santorini Volcano: Geological Society of London Memoir 19, 165 p.

Elkins Tanton, L.T., Grove, T.L., and Donnelly-Nolan, J., 2001, Hot, shallow mantle melting under the Cascades volcanic arc: Geology, v. 29, no. 7, p. 631–634, doi: 10.1130/0091-7613(2001)029<0631:HSMMUT>2.0.CO;2.

Entenmann, 1994, Magmatic evolution of the Nevados de Payachata complex and the petrogenesis of basaltic andesites in the Central Volcanic Zone of northern Chile [Ph.D. thesis]: Mainz, Johannes Gutenberg-Universität in Mainz, 188 p.

Francis, P.W., and Wells, G.L., 1988, Landsat Thematic Mapper observations of debris avalanche deposits in the central Andes: Bulletin of Volcanology, v. 50, p. 258–278, doi: 10.1007/BF01047488.

Frey, H.M., Lange, R.A., Hall, C.M., and Delgado-Granados, H., 2004, Magma eruption rates constrained by $^{40}Ar/^{39}Ar$ chronology and GIS for the Ceboruco–San Pedro volcanic field, western Mexico: Geological Society of America Bulletin, v. 116, no. 3–4, p. 259–276, doi: 10.1130/B25321.1.

Ginibre, C., Kronz, A., and Wörner, G., 2002a, High-resolution quantitative imaging of plagioclase composition using accumulated backscattered electron images: New constraints on oscillatory zoning: Contributions to Mineralogy and Petrology, v. 142, no. 4, p. 436–448.

Ginibre, C., Wörner, G., and Kronz, A., 2002b, Minor- and trace-element zoning in plagioclase: Implications for magma chamber processes at Parinacota volcano, northern Chile: Contributions to Mineralogy and Petrology, v. 143, no. 3, p. 300–315.

González Ferrán, O., 1995, Volcanes de Chile: Santiago, Chile, Instituto Geográfico Militar, 640 p.

Grove, T.L., and Kinzler, R.J., 1986, Petrogenesis of andesites: Annual Review of Earth and Planetary Sciences, v. 14, p. 417–454, doi: 10.1146/annurev.ea.14.050186.002221.

Grove, T.L., Parman, S.W., Bowring, S.A., Price, R.C., and Baker, M.B., 2002, The role of an H_2O-rich fluid component in the generation of primitive basaltic andesites and andesites from the Mt. Shasta region, N California: Contributions to Mineralogy and Petrology, v. 142, no. 4, p. 375–396.

Harford, C.L., Pringle, M.S., Sparks, R.S.J., and Young, S.R., 2002, The volcanic evolution of Montserrat using $^{40}Ar/^{39}Ar$ geochronology, *in* Druitt, T.H., and Kokelaar, B.P., eds., The Eruption of Soufriere Hills Volcano, Montserrat, from 1995 to 1999: Geological Society of London Memoir 21, p. 93–113.

Hawkesworth, C., George, R., Turner, S., and Zellmer, G., 2004, Time scales of magmatic processes: Earth and Planetary Science Letters, v. 218, no. 1–2, p. 1–16, doi: 10.1016/S0012-821X(03)00634-4.

Herron, E.M., 1972, Sea-floor spreading and Cenozoic history of east-central Pacific: Geological Society of America Bulletin, v. 83, no. 6, p. 1671–1691.

Hildreth, W., and Lanphere, M.A., 1994, Potassium-argon geochronology of a basalt-andesite-dacite arc system—The Mount Adams volcanic field, Cascade Range of southern Washington: Geological Society of America Bulletin, v. 106, no. 11, p. 1413–1429, doi: 10.1130/0016-7606(1994)106<1413:PAGOAB>2.3.CO;2.

Hildreth, W., and Moorbath, S., 1988, Crustal contributions to arc magmatism in the Andes of central Chile: Contributions to Mineralogy and Petrology, v. 98, no. 4, p. 455–489, doi: 10.1007/BF00372365.

Hildreth, W., Fierstein, J., and Lanphere, M., 2003a, Eruptive history and geochronology of the Mount Baker volcanic field, Washington: Geological Society of America Bulletin, v. 115, no. 6, p. 729–764, doi: 10.1130/0016-7606(2003)115<0729:EHAGOT>2.0.CO;2.

Hildreth, W., Lanphere, M.A., and Fierstein, J., 2003b, Geochronology and eruptive history of the Katmai volcanic cluster, Alaska Peninsula: Earth and Planetary Science Letters, v. 214, no. 1–2, p. 93–114, doi: 10.1016/S0012-821X(03)00321-2.

Hinners, T.A., Hughes, R., Outridge, P.M., Davis, W.J., Simon, K., and Woolard, D.R., 1998, Interlaboratory comparison of mass spectrometric methods for lead isotopes and trace elements in NIST SRM 1400 Bone Ash: Journal of Analytical Atomic Spectrometry, v. 13, no. 9, p. 963–970, doi: 10.1039/a803373k.

James, D.E., 1971, Plate tectonic model for evolution of central Andes: Geological Society of America Bulletin, v. 82, no. 12, p. 3325–3345.

Jicha, B.R., and Singer, B.S., 2006, Volcanic history and magmatic evolution of Seguam Island, Aleutian Island Arc, Alaska: Geological Society of America Bulletin, v. 118, no. 7–8, p. 805–822, doi: 10.1130/B25861.1.

Jicha, B.R., Singer, B.S., Beard, B.L., and Johnson, C.M., 2005, Contrasting timescales of crystallization and magma storage beneath the Aleutian Island arc: Earth and Planetary Science Letters, v. 236, no. 1–2, p. 195–210, doi: 10.1016/j.epsl.2005.05.002.

Jordan, T.E., Isacks, B.L., Allmendinger, R.W., Brewer, J.A., Ramos, V.A., and Ando, C.J., 1983, Andean tectonics related to geometry of subducted Nazca plate: Geological Society of America Bulletin, v. 94, no. 3, p. 341–361, doi: 10.1130/0016-7606(1983)94<341:ATRTGO>2.0.CO;2.

Kaplan, M.R., Ackert, R.P., Singer, B.S., Douglass, D.C., and Kurz, M.D., 2004, Cosmogenic nuclide chronology of millennial-scale glacial advances during O-isotope stage 2 in Patagonia: Geological Society of America Bulletin, v. 116, no. 3–4, p. 308–321, doi: 10.1130/B25178.1.

Koppers, A.A.P., 2002, ArArCALC—Software for $^{40}Ar/^{39}Ar$ age calculations: Computers & Geosciences, v. 28, no. 5, p. 605–619, doi: 10.1016/S0098-3004(01)00095-4.

Lanphere, M.A., and Dalrymple, G.B., 1976, Identification of excess ^{40}Ar by $^{40}Ar/^{39}Ar$ age spectrum technique: Earth and Planetary Science Letters, v. 32, no. 2, p. 141–148, doi: 10.1016/0012-821X(76)90052-2.

Leeman, W.P., 1983, The influence of crustal structure on compositions of subduction-related magmas: Journal of Volcanology and Geothermal Research, v. 18, no. 1–4, p. 561–588, doi: 10.1016/0377-0273(83)90026-4.

Lewis-Kenedi, C.B., Lange, R.A., Hall, C.M., and Delgado-Granados, H., 2005, The eruptive history of the Tequila volcanic field, western Mexico: Ages, volumes, and relative proportions of lava types: Bulletin of Volcanology, v. 67, no. 5, p. 391–414, doi: 10.1007/s00445-004-0377-3.

Lucassen, F., Becchio, R., Harmon, R., Kasemann, S., Franz, G., Trumbull, R., Wilke, H.G., Romer, R.L., and Dulski, P., 2001, Composition and density model of the continental crust at an active continental margin—The central Andes between 21 degrees and 27 degrees S: Tectonophysics, v. 341, no. 1–4, p. 195–223, doi: 10.1016/S0040-1951(01)00188-3.

McDougall, I., and Harrison, T.M., 1999, Geochronology and thermochronology by the $^{40}Ar/^{39}Ar$ method: New York, Oxford University Press, 269 p.

McMillan, N.J., Davidson, J.P., Wörner, G., Harmon, R.S., Moorbath, S., and Lopez-Escobar, L., 1993, Influence of crustal thickening on arc magmatism—Nevados de Payachata volcanic region, northern Chile: Geology, v. 21, no. 5, p. 467–470, doi: 10.1130/0091-7613(1993)021<0467:IOCTOA>2.3.CO;2.

Moreno, A., Giralt, S., Valero-Garcés, B., Sáez, A., Bao, R., Prego, R., Pueyo, J.J., González-Sampériz, P., Taberner, C., 2006, A 14 kyr record of the tropical Andes: The Lago Chungará sequence (18°S, northern Chilean Altiplano): Quaternary International, doi:10.1016/j.quaint.2006.10.020.

Müller, R.D., Roest, W.R., Royer, J.Y., Gahagan, L.M., and Sclater, J.G., 1997, Digital isochrons of the world's ocean floor: Journal of Geophysical Research–Solid Earth, v. 102, no. B2, p. 3211–3214, doi: 10.1029/96JB01781.

Ochs, F.A., III, and Lange, R.A., 1999, The density of hydrous magmatic liquids: Science, v. 283, no. 5406, p. 1314–1317, doi: 10.1126/science.283.5406.1314.

Petford, N., Cruden, A.R., McCaffrey, K.J.W., and Vigneresse, J.L., 2000, Granite magma formation, transport and emplacement in the Earth's crust: Nature, v. 408, no. 6813, p. 669–673, doi: 10.1038/35047000.

Phillips, D., and Onstott, T.C., 1988, Argon isotopic zoning in mantle phlogopite: Geology, v. 16, no. 6, p. 542–546, doi: 10.1130/0091-7613(1988)016<0542:AIZIMP>2.3.CO;2.

Pinel, V., and Jaupart, C., 2000, The effect of edifice load on magma ascent beneath a volcano: Philosophical Transactions of the Royal Society of London, ser. A, v. 358, no. 1770, p. 1515–1532.

Pinel, V., and Jaupart, C., 2004a, Likelihood of basaltic eruptions as a function of volatile content and volcanic

edifice size: Journal of Volcanology and Geothermal Research, v. 137, no. 1–3, p. 201–217, doi: 10.1016/j.jvolgeores.2004.05.010.

Pinel, V., and Jaupart, C., 2004b, Magma storage and horizontal dyke injection beneath a volcanic edifice: Earth and Planetary Science Letters, v. 221, no. 1–4, p. 245–262, doi: 10.1016/S0012-821X(04)00076-7.

Pinel, V., and Jaupart, C., 2005, Some consequences of volcanic edifice destruction for eruption conditions: Journal of Volcanology and Geothermal Research, v. 145, no. 1–2, p. 68–80, doi: 10.1016/j.jvolgeores.2005.01.012.

Renne, P.R., Swisher, C.C., Deino, A.L., Karner, D.B., Owens, T.L., and DePaolo, D.J., 1998, Intercalibration of standards, absolute ages and uncertainties in $^{40}Ar/^{39}Ar$ dating: Chemical Geology, v. 145, p. 117–152, doi: 10.1016/S0009-2541(97)00159-9.

Singer, B.S., Thompson, R.A., Dungan, M.A., Feeley, T.C., Nelson, S.T., Pickens, J.C., Brown, L.L., Wulff, A.W., Davidson, J.P., and Metzger, J., 1997, Volcanism and erosion during the past 930 ky at the Tatara–San Pedro complex, Chilean Andes: Geological Society of America Bulletin, v. 109, p. 127–142, doi: 10.1130/0016-7606(1997)109<0127:VAEDTP>2.3.CO;2.

Singer, B.S., Wijbrans, J.R., Nelson, S.T., Pringle, M.S., Feeley, T.C., and Dungan, M.A., 1998, Inherited argon in a Pleistocene andesite lava: $^{40}Ar/^{39}Ar$ incremental-heating and laser-fusion analyses of plagioclase: Geology, v. 26, no. 5, p. 427–430, doi: 10.1130/0091-7613(1998)026<0427:IAIAPA>2.3.CO;2.

Singer, B.S., Ackert, R.P., and Guillou, H., 2004, $^{40}Ar/^{39}Ar$ and K-Ar chronology of Pleistocene glaciations in Patagonia: Geological Society of America Bulletin, v. 116, no. 3–4, p. 434–450, doi: 10.1130/B25177.1.

Sisson, T.W., and Grove, T.L., 1993, Experimental investigations of the role of H_2O in calc-alkaline differentiation and subduction zone magmatism: Contributions to Mineralogy and Petrology, v. 113, no. 2, p. 143–166, doi: 10.1007/BF00283225.

Smith, J.A., Seltzer, G.O., Farber, D.L., Rodbell, D.T., and Finkel, R.C., 2005, Early local Last Glacial Maximum in the tropical Andes: Science, v. 308, no. 5722, p. 678–681, doi: 10.1126/science.1107075.

Smith, M.E., Singer, B., and Carroll, A., 2003, $^{40}Ar/^{39}Ar$ geochronology of the Eocene Green River Formation, Wyoming: Geological Society of America Bulletin, v. 115, no. 5, p. 549–565, doi: 10.1130/0016-7606(2003)115<0549:AGOTEG>2.0.CO;2.

Thompson, L.G., Davis, M.E., Mosley-Thompson, E., Sowers, T.A., Henderson, K.A., Zagorodnov, V.S., Lin, P.N., Mikhalenko, V.N., Campen, R.K., Bolzan, J.F., Cole-Dai, J., and Francou, B., 1998, A 25,000-year tropical climate history from Bolivian ice cores: Science, v. 282, no. 5395, p. 1858–1864, doi: 10.1126/science.282.5395.1858.

Thouret, J.C., Finizola, A., Fornari, M., Legeley-Padovani, A., Suni, J., and Frechen, M., 2001, Geology of El Misti volcano near the city of Arequipa, Peru: Geological Society of America Bulletin, v. 113, no. 12, p. 1593–1610, doi: 10.1130/0016-7606(2001)113<1593:GOEMVN>2.0.CO;2.

Ton-That, T., Singer, B., and Paterne, M., 2001, $^{40}Ar/^{39}Ar$ dating of latest Pleistocene (41 ka) marine tephra in the Mediterranean Sea: Implications for global climate records: Earth and Planetary Science Letters, v. 184, no. 3–4, p. 645–658, doi: 10.1016/S0012-821X(00)00358-7.

White, S.M., Crisp, J.A., and Spera, F.J., 2006, Long-term volumetric eruption rates and magma budgets: Geochemistry, Geophysics, Geosystems, v. 7, p. Q03010, doi: 10.1029/2005GC001002.

Wörner, G., Harmon, R.S., Davidson, J., Moorbath, S., Turner, D.L., Mcmillan, N., Nye, C., Lopez-Escobar, L., and Moreno, H., 1988, The Nevados de Payachata volcanic region (18°S/69°W, N. Chile): I. Geological, geochemical, and isotopic observations: Bulletin of Volcanology, v. 50, no. 5, p. 287–303, doi: 10.1007/BF01073587.

Wörner, G., Hammerschmidt, K., Henjes-Kunst, F., Lezaun, J., and Wilke, H., 2000a, Geochronology ($^{40}Ar/^{39}Ar$, K-Ar and He-exposure ages) of Cenozoic magmatic rocks from northern Chile (18′22°S): Implications for magmatism and tectonic evolution of the central Andes: Revista Geologica de Chile, v. 27, no. 2, p. 205–240.

Wörner, G., Lezaun, J., Beck, A., Heber, V., Lucassen, F., Zinngrebe, E., Rossling, R., and Wilke, H.G., 2000b, Precambrian and early Paleozoic evolution of the Andean basement at Belen (northern Chile) and Cerro Uyarani (western Bolivia Altiplano): Journal of South American Earth Sciences, v. 13, no. 8, p. 717–737, doi: 10.1016/S0895-9811(00)00056-0.

Manuscript Received 19 December 2005
Revised Manuscript Received 7 August 2006
Manuscript Accepted 26 September 2006

Printed in the USA